# KVN Status Report 2022

# Korean VLBI Network, Korea Astronomy and Space Science Institute

KVN group, Radio astronomy division



 $May\ 11,\ 2022$ 

# Contents

1	Intr	troduction					
2	KV	N System					
	2.1	Network					
		2.1.1 Array					
		2.1.2 UV coverage					
		2.1.3 Antenna location					
		2.1.4 Array Operation Center					
	2.2	Antennas					
		2.2.1 Optics and Driving performance					
		2.2.2 Antenna beam size and Aperture efficiency					
		2.2.3 Gain Curve					
		2.2.4 Beam pattern					
		2.2.5 Antenna pointing accuracy					
		2.2.6 Beam alignment					
		2.2.7 Skylines					
	2.3	Receiver					
		2.3.1 Quasi-optics					
		2.3.2 Block diagram					
		2.3.3 Frequency range					
		2.3.4 Receiver noise temperature					
		2.3.5 System temperatures with wide-band frequencies					
	2.4	Digital Process					
		2.4.1 Digital filter mode					
		2.4.2 Signal processing mode of OCTAD					
		2.4.3 Recorders					
		2.4.4 Spectrometers for Single-dish observation					
		2.4.5 Correlator					
	2.5	Calibration					
		2.5.1 Amplitude calibration					
	2.6	KVN geodetic VLBI measurement					
3	Obs	serving proposal 26					
	3.1	Observing mode					
	3.1	3.1.1 Multi-frequency observation					
		3.1.2 Fast position switching observation					
		3.1.3 2 Gbps/4 Gbps/8 Gbps observation modes (NEW!)					
	3.2	Angular resolution					
	3.3	Baseline sensitivity					
	3.4	System temperature					
	3.5 Astrometric observation						

4 Observation and Data Reduction					
	4.1	Preparation of observation and correlation	27		
		4.1.1 General information	27		
		4.1.2 Observation	28		
		4.1.3 Correlation	29		
	4.2	Data reduction	29		
		4.2.1 VLBI data reduction with AIPS	29		
	4.3	Correlator status	29		
		4.3.1 Daejeon Correlator	29		
		4.3.2 Correlation Processing	32		
		4.3.3 Performance of Daejeon Correlator (Continuum/Spectral-line)	33		
		4.3.4 Two-layer problem had been solved	44		
	4.4	Further information			

# List of Tables

1	Geographic locations of KVN Antennas
2	KVN antenna positions in geocentric coordinate system
3	KVN antenna optics specifications
4	Beam size and efficiency of each KVN antenna
5	Coefficients of normalized gain curves
6	KVN Antenna Pointing Accuracy
7	AZ/EL beam offset with respect to the 86 GHz LCP beam
8	Frequency range of the KVN receiver
9	KVN receiver noise temperature
10	System temperatures $(T_{\text{sys}})$ with wide-band frequencies
11	KVN digital filter mode
12	KVN OCTAD mode
13	Available mode of the GPU spectrometer at KTN and KUS
14	Available mode of the GPU spectrometer at KYS
15	Correlation mode of the KJCC
16	Angular resolutions at each KVN baseline and frequency
17	Baseline sensitivity of the KVN
18	Specification of Daejeon Correlator
19	Observation experiments list
20	Contact staffs
List	of Figures
1	Korean VLBI Network (KVN)
2	Simulated UV-coverage of K- (red) and Q- (blue) bands
3	Normalized gain curves of four bands (22, 43, 86, 129 GHz) at each KVN
	antenna
4	Beam patterns at Yonsei antenna. Top panel: Jupiter at 22 GHz (left) and
	43 GHz (right), Bottom panel: Venus at 86 GHz (left) and 129 GHz (right) 1
5	The residual of pointing model at 43 GHz (KYS, KUS, KTN, from top to
	The residual of pointing model at 43 GHz (KYS, KUS, KTN, from top to bottom)
6	The residual of pointing model at 43 GHz (KYS, KUS, KTN, from top to bottom)
6 7	The residual of pointing model at 43 GHz (KYS, KUS, KTN, from top to bottom)
6 7 8	The residual of pointing model at 43 GHz (KYS, KUS, KTN, from top to bottom)
6 7 8 9	The residual of pointing model at 43 GHz (KYS, KUS, KTN, from top to bottom)
6 7 8 9 10	The residual of pointing model at 43 GHz (KYS, KUS, KTN, from top to bottom)
6 7 8 9 10 11	The residual of pointing model at 43 GHz (KYS, KUS, KTN, from top to bottom)
6 7 8 9 10	The residual of pointing model at 43 GHz (KYS, KUS, KTN, from top to bottom)
6 7 8 9 10 11	The residual of pointing model at 43 GHz (KYS, KUS, KTN, from top to bottom)
6 7 8 9 10 11	The residual of pointing model at 43 GHz (KYS, KUS, KTN, from top to bottom)
6 7 8 9 10 11	The residual of pointing model at 43 GHz (KYS, KUS, KTN, from top to bottom)

14	Data reduction flow chart with AIPS	30
15	Block diagram of Daejeon Correlator	31
16	Daejeon Correlator installed at Korea-Japan Correlation Center	32
17	Spectrum shape of 16 IF continuum for KYS-KUS baseline	34
18	Variation pattern of gain amplitude for all stations with $9^{th}$ IF. Left (Daejeon	
	Correlator), Right (DiFX)	34
19	SNR, Delay, Rate after FRING for 1 <sup>st</sup> IF of the KYS. Upper (Daejeon Cor-	
	relator), Bottom (DiFX)	35
20	Closure phase after fringe fitting. Upper (Daejeon Correlator), Bottom (DiFX).	35
21	Spectrum shape after fringe fitting. Left (Daejeon Correlator), Right (DiFX).	36
22	2-dimensional image map using Difmap. Left (Daejeon Correlator), Right	
	(DiFX)	36
23	Flux density according to UV-distance. Left (Daejeon Correlator), Right	
	(DiFX)	37
24	Spectrum shape of 8-IFs continuum for KYS-KUS baseline. Left (Daejeon	
	Correlator), Right (DiFX)	37
25	Variable characteristics of gain amplitude for each IF of KVNTN. Left (Dae-	
		38
26	SNR, Delay, Rate after FRING for each IF of KTN. Left (Daejeon Correlator),	
	Right (DiFX)	39
27	Closure phase after fringe fitting. Upper (Daejeon Correlator), Bottom (DiFX)	40
28	Closure phase after fringe fitting. Upper (Daejeon Correlator), Bottom (DiFX)	40
29	Closure phase after fringe fitting. Upper (Daejeon Correlator), Bottom (DiFX)	40
30	2-dimensional image map using Difmap. Left (Daejeon Correlator), Right	
	(DiFX)	41
31	Spectrum shape of 9th IF of KYS and KUS baseline	41
32	Fringe fitting result of 3C345 as calibrator source	42
33	Fringe fitting result of Sgr B2(M) as maser source, and this figure shows SNR	
	based on the KTN	42
34	Spectrum shape after fringe fitting, Dopper effect, and amplitude calibration.	43
35	UV coverage (Left) and UV plot (Right) of Sgr B2(M). UV plot looks like	
	Gaussian distribution, but KVN-only baseline seems to be flat	43
36	2-dimensional image map using AIPS. Left (Daejeon Correlator), Right (DiFX).	44
37	Example of multi-channel image. Image result for each 261th–290th channel.	45
38	(Left) Before: abnormal shape with two-layer pattern, (Right) After: ordinary	
	(as expected) shape in Gain amplitude plot (KYS, R11027B)	45

# 1 Introduction

Korean VLBI Network (KVN) is the only VLBI facility in Korea. It consists of three 21-m radio telescopes, which are located in Seoul (Yonsei Univ.), Ulsan (Univ. of Ulsan), and Jeju island (Tamna Univ.), and produce an effective spatial resolution equivalent to that of a 500-km radio telescope. The KVN is still small, compared to American and European VLBI networks such as VLBA and EVN. To overcome this shortcoming, KASI has developed innovative multi-frequency band receiver systems, observing four different frequencies, i.e., 22, 43, 86, 129 GHz, simultaneously. With this capability, The KVN will provide opportunities to study the formation and death processes of stars, the structure and dynamics of our Galaxy, the nature of Active Galactic Nuclei, and so on at milli-arcsecond resolutions [1].

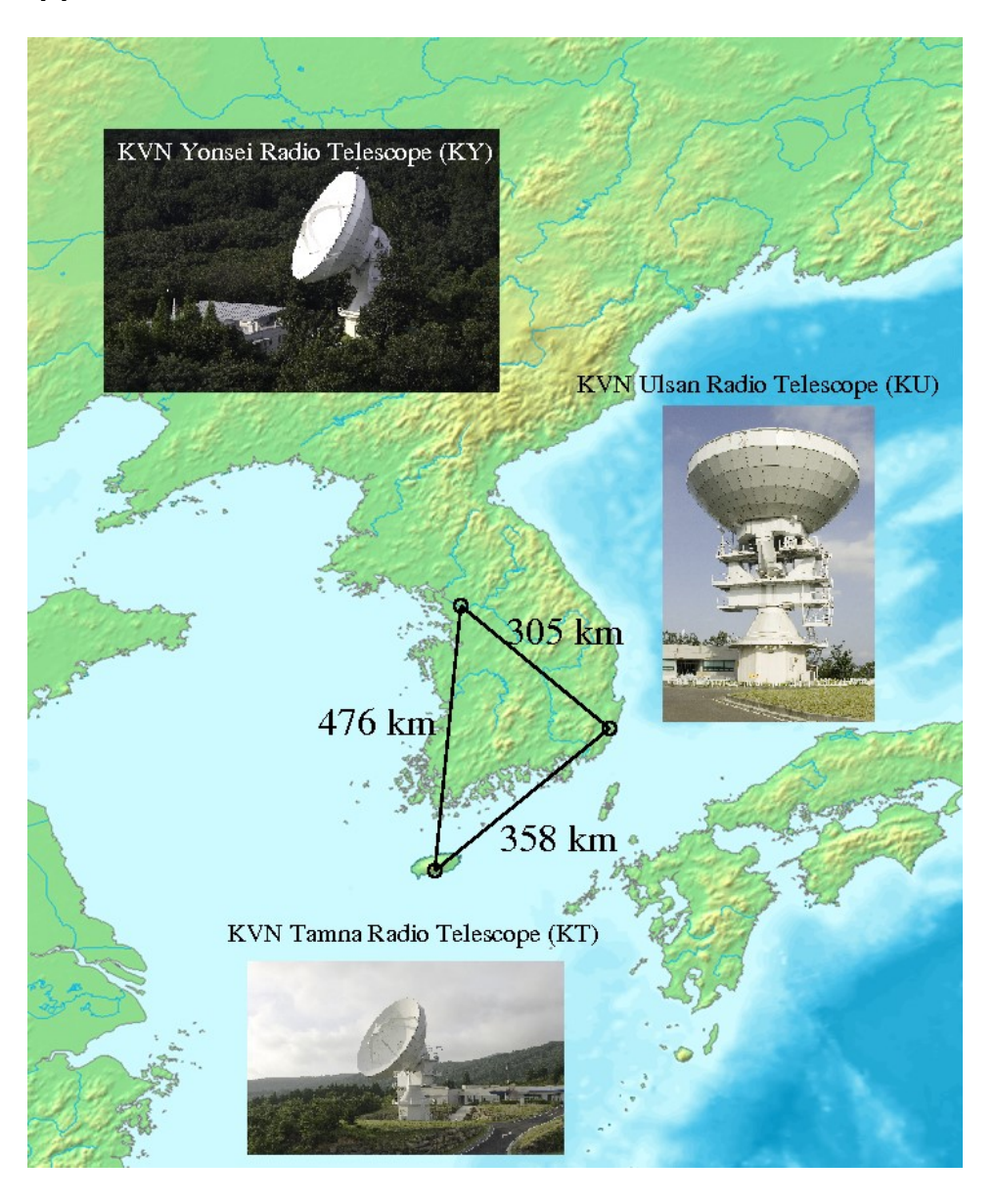


Figure 1: Korean VLBI Network (KVN)

# 2 KVN System

# 2.1 Network

# 2.1.1 Array

The Korean VLBI Network (KVN) is a three-element Very Long Baseline Interferometry (VLBI) network in Korea, which is dedicated to VLBI observations at millimeter wavelengths. Three 21-m radio telescopes are located in Seoul, Ulsan, and Jeju island, Korea; KVN Yonsei Radio Telescope (hereafter KYS), KVN Ulsan Radio Telescope (hereafter KUS), and KVN Tamna Radio Telescope (hereafter KTN). The baseline lengths are in a range of 305-476km. All antennas have the same design (Figure 1).

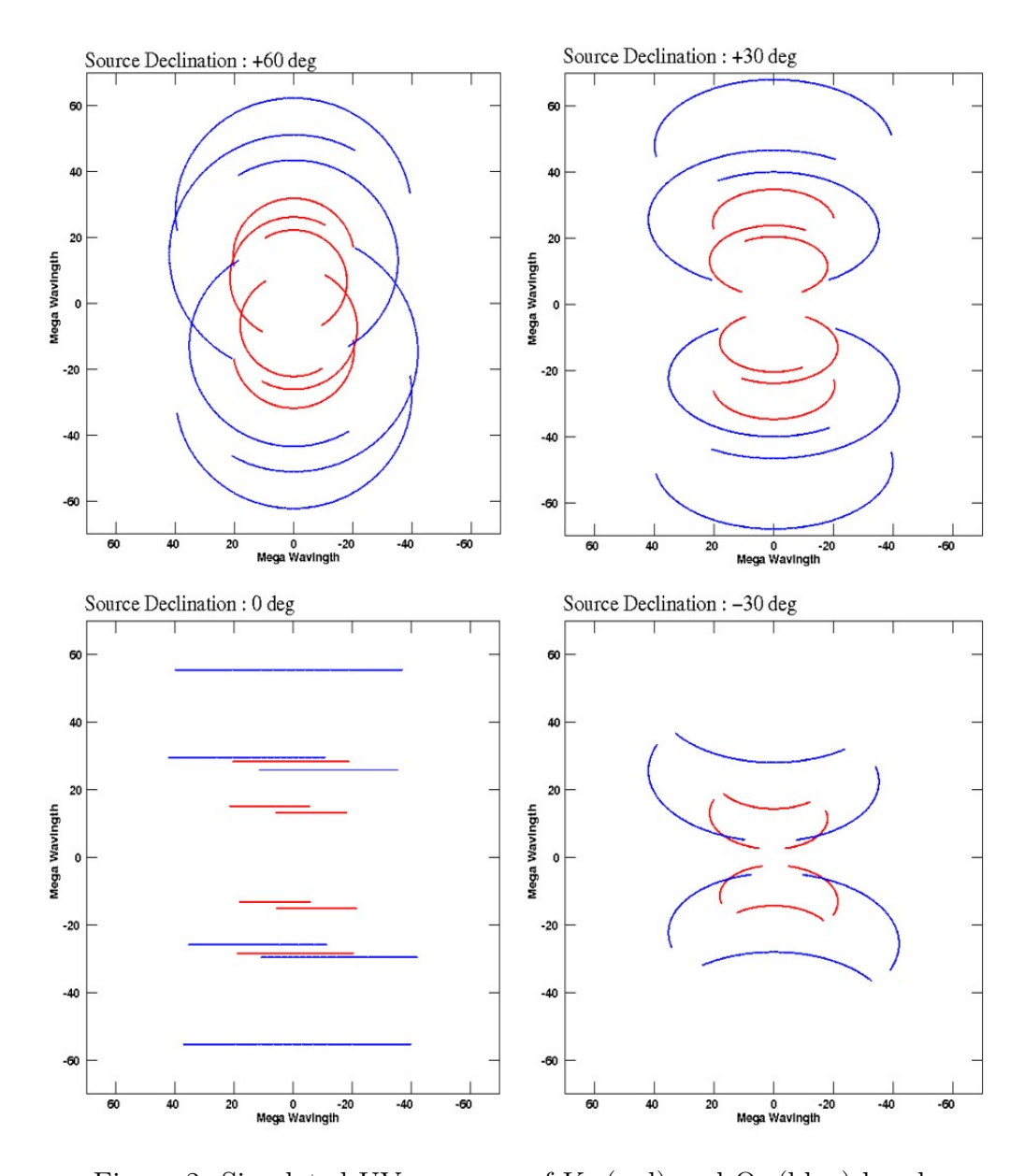


Figure 2: Simulated UV-coverage of K- (red) and Q- (blue) bands

# 2.1.2 UV coverage

As shown in Figure 2, we present the simulated UV-coverage of KVN at K- (red) and Q-band (blue) for sources with different declination, +60, +30, 0, and -30 degrees, that were observed for 12 hours.

#### 2.1.3 Antenna location

Table 1 shows the measured coordinates of KVN antennas, and Table 2 gives the geographic locations of three stations of the KVN, ordered from North through South. All locations of KVN antennas are measured with a GPS. Antenna positions of the KVN are regularly monitored both with a GPS and geodetic VLBI observations in collaboration with VERA.

Antenna	Latitude	Longitude	Elevation
	(° ′ ″)	(° ′ ″)	(m)
KYS	126:56:27.4	37:33:54.9	139
KUS	129:14:59.3	35:32:44.2	170
KTN	126.27.34 4	33.17.20.9	452

Table 1: Geographic locations of KVN Antennas

Table 2: KVN antenna positions in geocentric coordinate system

Antenna	$\mathrm{MJD}^a$	X (m)	Y (m)	Z (m)
KYS	58485	-3042281.0183	4045902.6730	3867374.3296
KUS	58485	-3287268.6453	4023450.1367	3687379.9886
KTN	58485	-3171731.6665	4292678.5393	3481038.7880

<sup>&</sup>lt;sup>a</sup> The epoch of the coordinates is January 1, 2019.

### 2.1.4 Array Operation Center

The KVN antennas can be controlled remotely from the Array Operation Center (AOC) in East Asia VLBI Center, KASI, Daejeon. The KVN stations are connected with the AOC through a high-speed dedicated network, a.k.a. KREONET (Korea Research Environment Open NETwork). Since the KVN antennas can be operated remotely from the AOC, the AOC operator must know the weather conditions which could influence the VLBI data quality during observations. Therefore, a weather station is located at each KVN observatory, sending information on the air temperature, dew point, wind speed, wind direction, and air pressure to the AOC.

#### 2.2 Antennas

### 2.2.1 Optics and Driving performance

The KVN antennas are designed to be a shaped-Cassegrain-type antenna with an altitude-

azimuth mount. The telescope has the main reflector of 21-m diameter with a focal length of 6.78-m. The main reflector consists of 200 aluminum panels with a manufacturing surface accuracy of about 65  $\mu$ m. The slewing speed of the main reflector is 3 °/second, which enables fast position-switching observations. The sub-reflector position, tilt, and tip are remotely controlled and modeled to compensate for the gravitational deformation of the main reflector and for the sagging-down of the sub-reflector itself. The characteristics of the antenna optics are summarized in Table 3.

Table 3: KVN antenna optics specifications

Main reflector	Parameters
(Axisymmetric Paraboloid)	
Diameter	$D = 21.03 \mathrm{m}$
Focal length	$f = 6.78 \mathrm{m}$
Focal ratio	f/D = 0.32
Panels manufacturing accuracy	$65\mu\mathrm{m}$
Alignment surface accuracy	$50 ext{-}54\mu\mathrm{m}$
Sub-reflector (Hyperboloid) diameter	Parameters
Diameter	$d = 2.25 \mathrm{m}$
Manufacturing surface accuracy	$50\mu\mathrm{m}$
Expected total surface accuracy	$124\mu\mathrm{m}$ at EL $48^\circ$
Slewing speed	3  °/sec
Slewing acceleration	$3 \text{ °/sec}^2$
Operating range	Az.: $\pm 270^{\circ}$ , El.: $0^{\circ}-90^{\circ}$

#### 2.2.2 Antenna beam size and Aperture efficiency

For all three KVN telescopes, antenna panel adjustment process were carried out from December 2021 to March 2022. As a result, the surface accuracy of three telescopes were improved to 70 (KYS), 72 (KUS), and 70 (KTN)  $\mu$ m, respectively, and accordingly, HPBW and aperture efficiency were also remeasured. Table 4 shows measurement results of HPBW, aperture efficiency, and main-beam efficiency at 22.235 (K), 43.122 (Q), 86.243 (W), and 129.363 (D) GHz. The values of the K- and Q-bands were obtained through observations toward Jupiter, while those of the W- and D-bands were obtained through observations toward Mars. Jupiter's brightness temperatures, applied to the above calculations, are 136.2 and 154.8 K at K- and Q-bands, respectively. The Mars brightness modeling values presented on its web page<sup>1</sup> are applied to the calculations for W- and D-bands.

#### • Elevation dependency

Aperture efficiency varies with elevation. The elevation dependency of the KVN antennas represented as a gain curve is described in the next section. Those in Column (4) are the maximum values.

<sup>1</sup>https://lesia.obspm.fr/perso/emmanuel-lellouch/mars/

Table 4: Beam size and efficiency of each KVN antenna

Site	Band (L, R)	HPBW	Aperture efficiency	Beam efficiency	$C.F.^a$
	(GHz)	(arcsec)	(%)	(%)	(Jy/K)
(1)	(2)	(3)	(4)	(5)	(6)
KYS	22 (L)	131	64	56	12.41
	22 (R)	130	68	58	11.68
	43 (L)	67	69	59	11.56
	43 (R)	67	69	59	11.60
	86 (L)	32	51	38	15.60
	86 (R)	32	51	38	15.60
	129 (L)	25	41	37	19.66
	129 (R)	24	41	37	19.66
KUS	22 (L)	129	69	58	11.52
	22 (R)	128	71	58	11.26
	43 (L)	65	65	54	12.31
	43 (R)	66	69	56	11.58
	86 (L)	32	59	46	13.54
	86 (R)	31	61	45	13.17
	129 (L)	23	53	47	15.04
	129 (R)	22	51	44	15.49
KTN	22 (L)	128	70	57	11.33
	22 (R)	129	74	61	10.78
	43 (L)	64	64	49	12.53
	43 (R)	63	65	50	12.22
	86 (L)	34	55	47	14.60
	86 (R)	34	54	46	14.70
	129 (L)	25	41	41	20.10
<i>a</i> . 1:	129 (R)	24	41	40	19.83

<sup>&</sup>lt;sup>a</sup> indicates the conversion factor between the antenna temperature and the flux density.

# • Frequency dependency of beam efficiency

Beam efficiency varies with beam size. The measured HPBWs are tabulated in Column (3), which are almost the same as the theoretical one (=  $\lambda$ /D of the antenna). To get a beam efficiency at 90 GHz, you have to multiply (86/90)<sup>2</sup> to that at 86 GHz.

# • Quantization correction of single-dish spectrum data

In case you are reducing single-dish spectrum data, it has to be multiplied by a factor of 1.25 before applying efficiency corrections. This is to compensate for the effect of the digital filter and spectrometer.

- Parameters of Table 4 can be applied for the following observing season;
  - KYS: from February 2022 now
  - KUS: from March 2022 now

#### 2.2.3 Gain Curve

The main reflector panels of KVN antennas were installed to give the maximum gain at the elevation angle of 48°. The sagging of the sub-reflector and the deformation of the main reflector by gravity with elevation results in degradation of antenna aperture efficiency with elevation. To compensate for this effect, a hexapod is utilized to adjust the sub-reflector position in KVN antennas. Although the hexapod correction reduces significantly the dependence of aperture efficiency with elevation, the degradation still appears evidently at a higher frequency. Figure 3 shows the elevation dependency of antenna aperture efficiency of the KVN 21-m radio telescopes measured by observing Venus, Jupiter, or 3C84 using the observation mode of "Cross Scan".

We derived a normalized gain curve which has the following form:  $G\_norm = A0 \cdot EL^2 + A1 \cdot EL + A2$ , where EL is the elevation in degree, by fitting a second-order polynomial to the data and normalizing the fitted function with its maximum value. The fitted parameters are summarized in Table 5.

It is expected that the antenna panel alignment will be much flatter than before, due to the antenna mirror adjustment process carried out from December 2021 to March 2022. Therefore, it is necessary to perform the gain curve measurement again. This part will be implemented and updated in middle of 2022.

#### 2.2.4 Beam pattern

The optics of the KVN antenna is a shaped-Cassegrain type of which the main reflector and sub-reflector are shaped to have a uniform illumination pattern on an aperture plane. Because of the uniform illumination, KVN antennas can get higher aperture efficiency than the value of typical Cassegrain type antennas. However, a higher side-lobe level is inevitable. Figure 4 presents OTF images of Jupiter at 22 and 43 GHz, and Venus at 86 and 129 GHz measured at Yonsei antenna, respectively. The map size is  $12' \times 10'$  for 22 and 43 GHz, and  $3.5' \times 3'$  for 86 and 129 GHz. The first sidelobe pattern is visible. Typical sidelobe levels of KVN antennas are  $13-14\,\mathrm{dB}$ .

#### 2.2.5 Antenna pointing accuracy

A sample of late-type evolved stars has been used to improve the pointing accuracy of the telescope since 2009. In Table 6, we present the accuracy of pointing models for three KVN radio telescopes established in May and September 2021. The root mean square (rms) of the residual pointing offsets between the observations and the pointing models are listed in total, azimuth, and elevation for each epoch and telescope, respectively ( $Total\ Error = Sqrt(Az\_Error^2 + El\_Error^2)$ ). The residual of the pointing model of each KVN telescope is shown in Figure 5.

In the case of observations during the daytime, especially at sunrise and sunset, the pointing observations must be conducted out at least every hour for maintaining the pointing accuracy to be less than 6 arcsecond in rms.

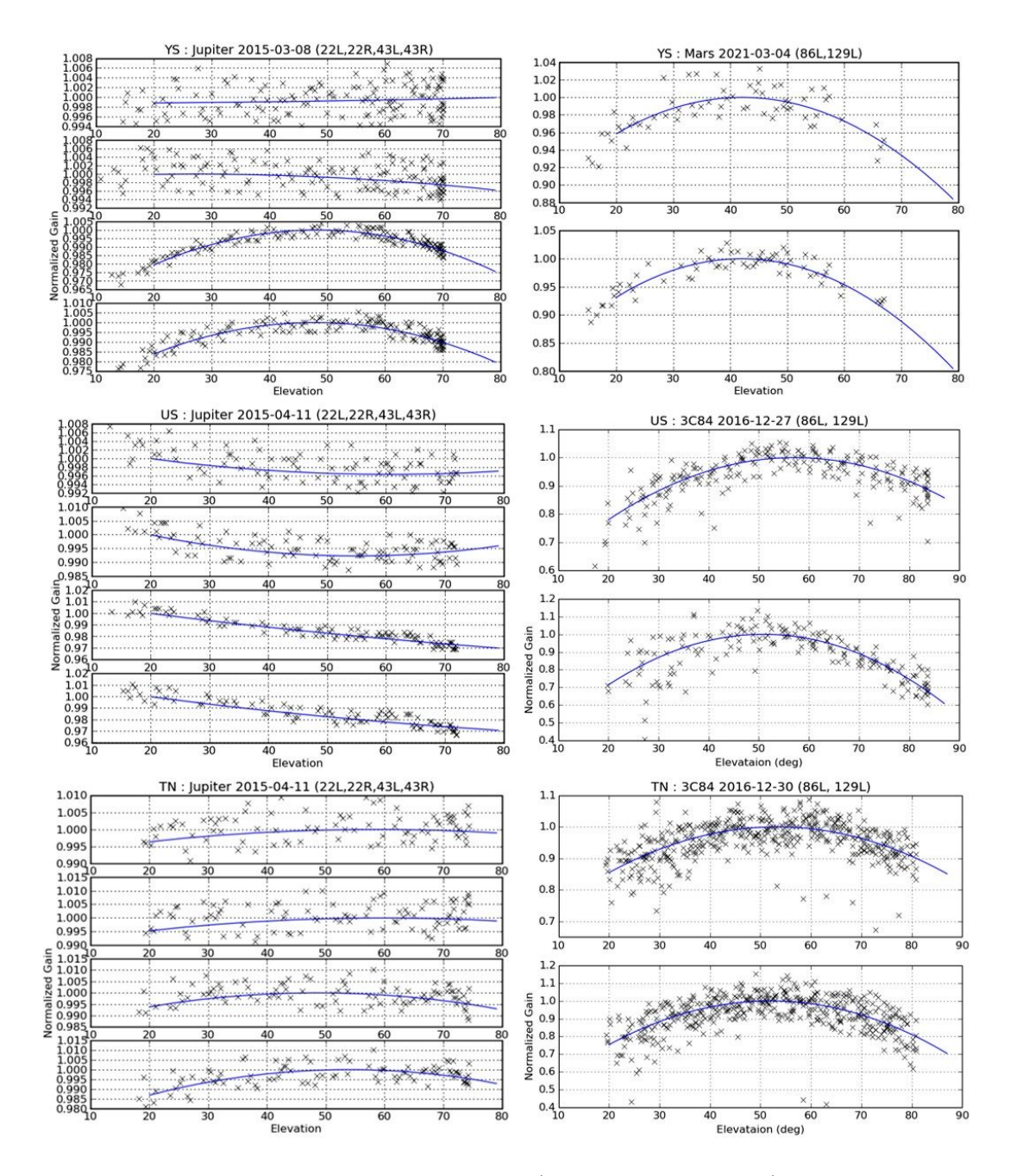


Figure 3: Normalized gain curves of four bands (22, 43, 86, 129 GHz) at each KVN antenna

# 2.2.6 Beam alignment

For the simultaneous observations of the 4 frequency bands, the quasi-optics should be aligned so that all 4 beams are directed at the same position in the sky. Table 7 shows pointing offsets of the other frequency bands to the center of the 86 GHz LCP beam. The relative offsets were obtained from the result of the Cross Scan after the alignment. As result, the 22 GHz beam is aligned within 5 arcseconds, while those of 129 and 43 GHz are aligned within 3 arcseconds.

Table 5: Coefficients of normalized gain curves

Site	Band (L, R)	A0	A1	A2
KYS	22 (L)	1.230E - 07	6.930E - 06	9.990E - 01
	22 (R)	-1.320E-06	6.720E - 05	9.990E - 01
	$43 \; (L)$	-2.560E-05	2.470E - 03	9.410E - 01
	43 (R)	-2.080E-05	1.990E - 03	9.520E - 01
	86 (L)	-8.482E - 05	7.136E - 03	8.499E - 01
	86 (R)	-8.482E - 05	7.136E - 03	8.499E - 01
	129 (L)	-1.421E-04	1.192E - 02	7.501E - 01
	129 (R)	-1.421E-04	1.192E - 02	7.501E - 01
KUS	22 (L)	2.170E - 06	-2.630E-04	1.000E+00
	22 (R)	6.170E - 06	-6.780E - 04	1.010E+00
	$43 \; (L)$	2.030E - 06	-7.050E-04	1.010E+00
	43 (R)	2.860E - 06	-7.720E-04	1.010E+00
	86 (L)	-1.600E-04	1.820E - 02	4.790E - 01
	86 (R)	-1.600E-04	1.820E - 02	4.790E - 01
	129 (L)	-3.000E-04	3.060E - 02	2.220E - 01
	129 (R)	-3.000E-04	3.060E - 02	2.220E - 01
KTN	22 (L)	-2.395E-06	2.807E - 04	9.918E - 01
	22 (R)	-2.938E-06	3.517E - 04	9.895E - 01
	43 (L)	-7.522E-06	7.301E - 04	9.823E - 01
	43 (R)	-1.128E-05	1.217E - 03	9.672E - 01
	86 (L)	-1.110E-04	1.173E - 02	6.899E - 01
	86 (R)	-1.159E-04	1.231E-02	6.729E - 01
	129 (L)	-1.994E-04	2.161E - 02	4.143E - 01
	129 (R)	-1.957E - 04	2.132E - 02	4.193E - 01

Table 6: KVN Antenna Pointing Accuracy

Site	Total	Azimuth	Elevation	Frequency	Date
	(arcsec)	(arcsec)	(arcsec)	(GHz)	
KYS	5.60	3.24	4.57	43	Sep. 20 2021
KUS	5.32	2.75	4.55	43	May 24 2021
KTN	4.74	2.85	3.79	43	Sep. 20 2021

In the case of the KUS, the beam alignment process was re-performed on September 30, 2021. In this work, other frequency beams were aligned based on the  $86\,\mathrm{GHz}$  RCP beam (Table 7).

# 2.2.7 Skylines

Blockages due to the nearby buildings, trees, and mountains determine skylines, which is the observable elevation limit with azimuth below which we cannot see the sky. Figure 6

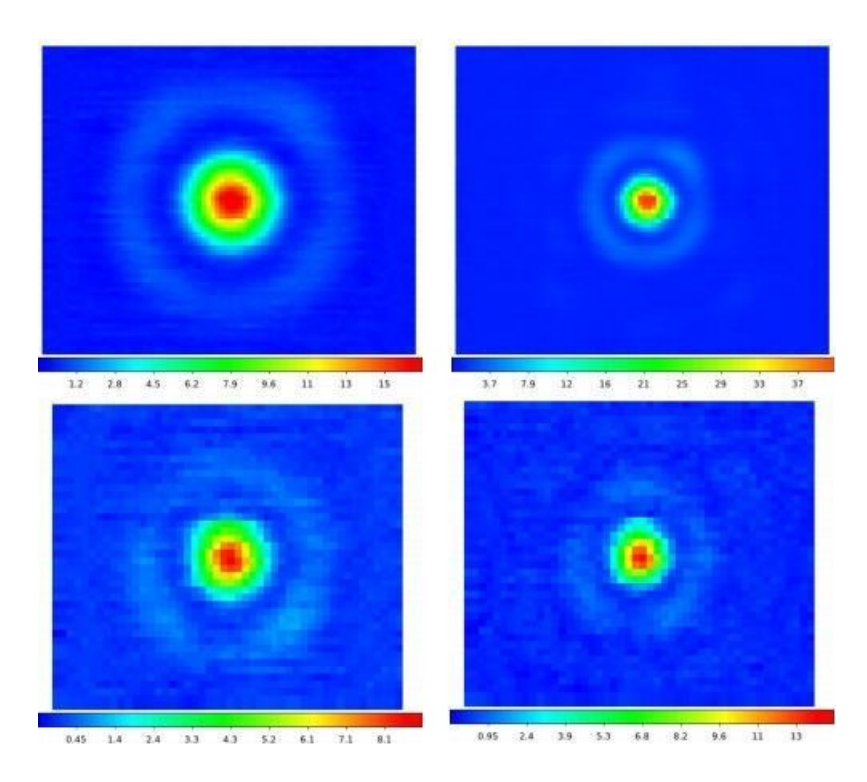


Figure 4: Beam patterns at Yonsei antenna. Top panel: Jupiter at 22 GHz (left) and 43 GHz (right), Bottom panel: Venus at 86 GHz (left) and 129 GHz (right).

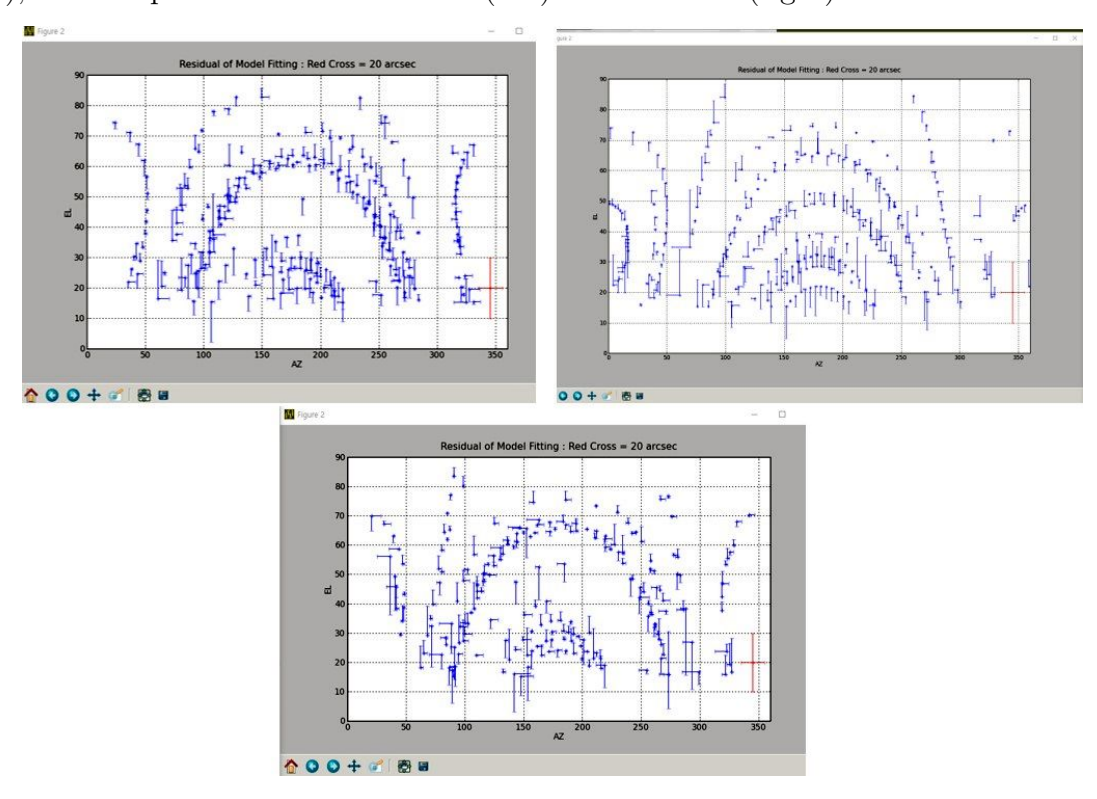


Figure 5: The residual of pointing model at 43 GHz (KYS, KUS, KTN, from top to bottom)

Table 7: AZ/EL beam offset with respect to the 86 GHz LCP beam

Site	Band (L, R)	Az. offset	El. offset
	(GHz)	(arcsec)	(arcsec)
KYS	22 (L)	$-0.8 (\pm 0.4)$	$-0.4 (\pm 0.4)$
	22 (R)	$-1.7 \ (\pm 0.4)$	$-0.9 \ (\pm 0.4)$
	$43 \; (L)$	$+1.1 \ (\pm 0.3)$	$-0.9 \ (\pm 0.2)$
	43 (R)	$+0.4 (\pm 0.4)$	$-1.3 \ (\pm 0.3)$
	86 (L)		
	86 (R)	$+2.2 \ (\pm 0.5)$	$0.0 \ (\pm 0.6)$
	129 (L)	$-2.8 \ (\pm 0.5)$	$+0.4 \ (\pm 0.6)$
	129 (R)	$-4.0 \ (\pm 0.5)$	$-0.3 \ (\pm 0.8)$
$\mathrm{KUS}^a$	22 (L)	$-0.8 \ (\pm 0.5)$	$+2.0\ (\pm0.6)$
	22 (R)	$-1.6 (\pm 1.4)$	$+3.1 \ (\pm 0.1)$
	$43 \; (L)$	$-0.5 \ (\pm 0.2)$	$+0.4 (\pm 0.1)$
	43 (R)	$-1.0 \ (\pm 0.0)$	$+0.3 \ (\pm 0.0)$
	86 (L)	$-1.4 (\pm 0.1)$	$-0.1 \ (\pm 0.1)$
	86 (R)		
	129 (L)	` /	$+1.5 \ (\pm 0.3)$
	129 (R)	$-1.3 \ (\pm 0.1)$	$+1.1 \ (\pm 0.4)$
KTN	22 (L)	-2.6	+0.8
	22 (R)	-3.6	-0.1
	$43 \; (L)$	+0.3	-2.5
	43 (R)	+0.1	-1.8
	86 (L)		
	86 (R)	+2.1	0.0
	129 (L)	+2.0	-1.2
	129 (R)	+0.8	-1.4

<sup>&</sup>lt;sup>a</sup> was performed on September 30, 2021.

shows skylines of KVN sites measured in 2014.

# 2.3 Receiver

### 2.3.1 Quasi-optics

The KVN has the unique capability to observe four frequency bands [2], simultaneously. KVN quasi-optics are designed to enable this multi-frequency observation. Figure 7 shows the layout of quasi-optics and receivers viewing from the sub-reflector side. The quasi-optics system splits one signal from the sub-reflector into four using three dichroic low-pass filters marked as LPF1, LPF2, and LPF3 in the figure. The split signals into four different frequency bands are guided to corresponding receivers.

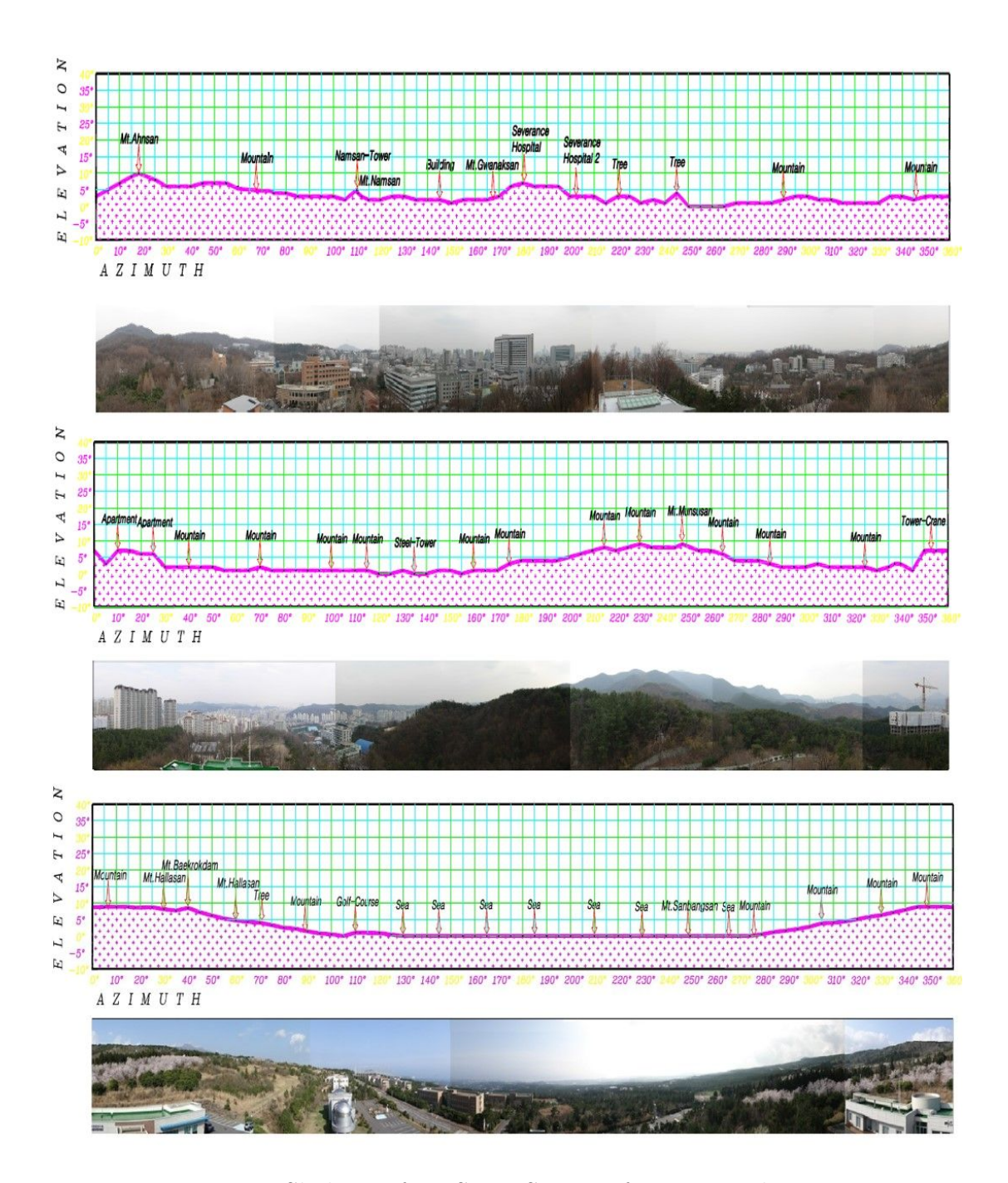


Figure 6: Skylines of KYS, KUS, KTN from top to bottom

# 2.3.2 Block diagram

The 22 (K), 43 (Q), and 86 (W) GHz band receivers are cooled HEMT receivers and the 129 (D) GHz band receiver is an SIS mixer receiver [3]. All receivers receive dual-circular-polarization signals. Among eight signals (four dual-polarization signals), four signals selected by the IF selector are down-converted to the input frequency band of the sampler. The samplers digitize signals into 2-bit data streams with four quantization levels. The sampling rate is 1024 Mega samples per second resulting in a 2 Gbps data rate (2-bit  $\times$ 

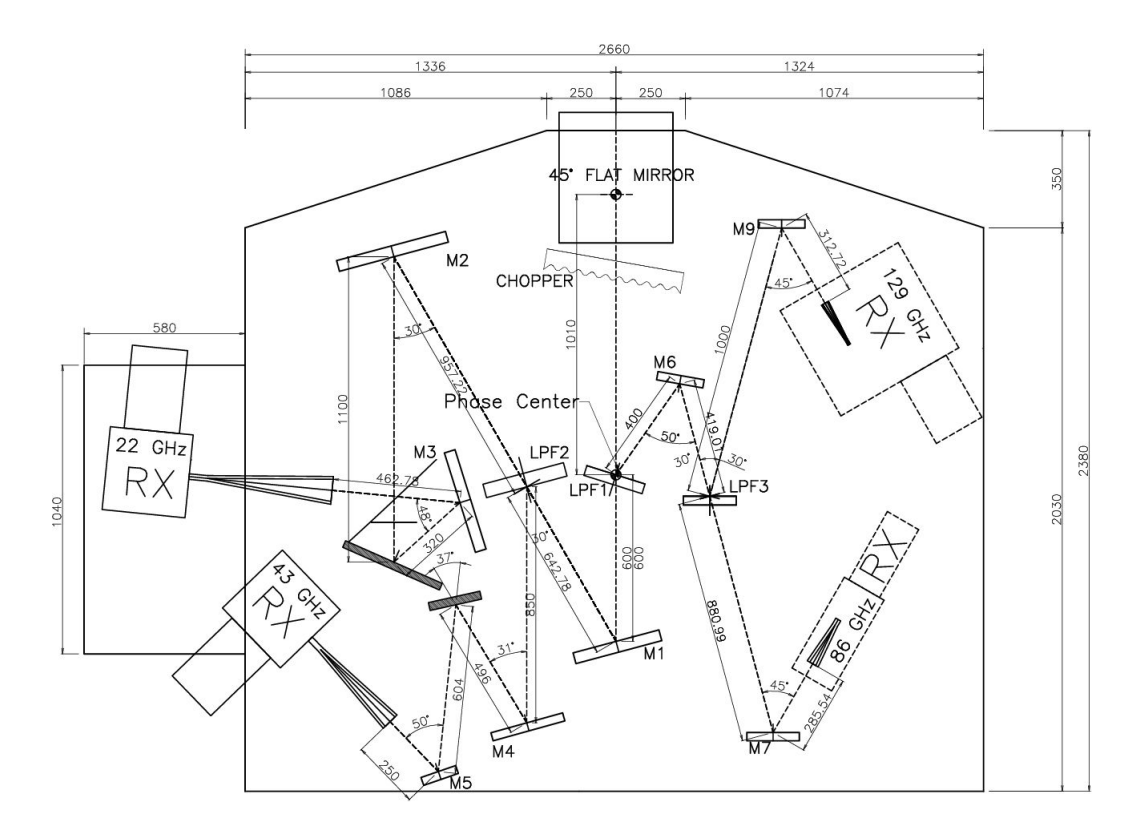


Figure 7: KVN multi-frequency receiving system

1024 Mega per second) and 512 MHz frequency bandwidth. In total, we can get 4 streams of 512 MHz bandwidth (2 Gbps data rate) simultaneously, which means that the total rate is 8 Gbps.

New wide-band VLBI backends including OCTAD, Mark6, and GPU spectrometer are introduced for wide-band operation. They are indicated in the red box of Figure 8. The OCTAD consists of four analog-digital converters, digital signal processing modules, and VDIF formatter. It digitizes four IF signals and makes signal processing for digital down-conversion and filtering. Combining OCTAD and ADS1K+Fila10G, all eight IF signals (four dual-polarization signals) can be obtained at the same time. The OCTAD has four 10 GbE outputs with which we can get a maximum 32 Gbps aggregated data rate.

#### 2.3.3 Frequency range

The instantaneous bandwidth of the 1st IF of each receiver is limited to 8 GHz by the band-pass filter. Table 8 shows the frequency range of each receiver. Q- and W-bands are divided into two frequency ranges. The low (high) frequency ranges of the Q-band receiver is from 35 (42) to 42 (50) GHz. The low (high) frequency ranges of the W-band receiver is from 85 (100) to 100 (116) GHz. Low- and high-frequency bands of the same polarization cannot be observed at the same time. Note that the D-band receiver has 2 GHz IF bandwidth.

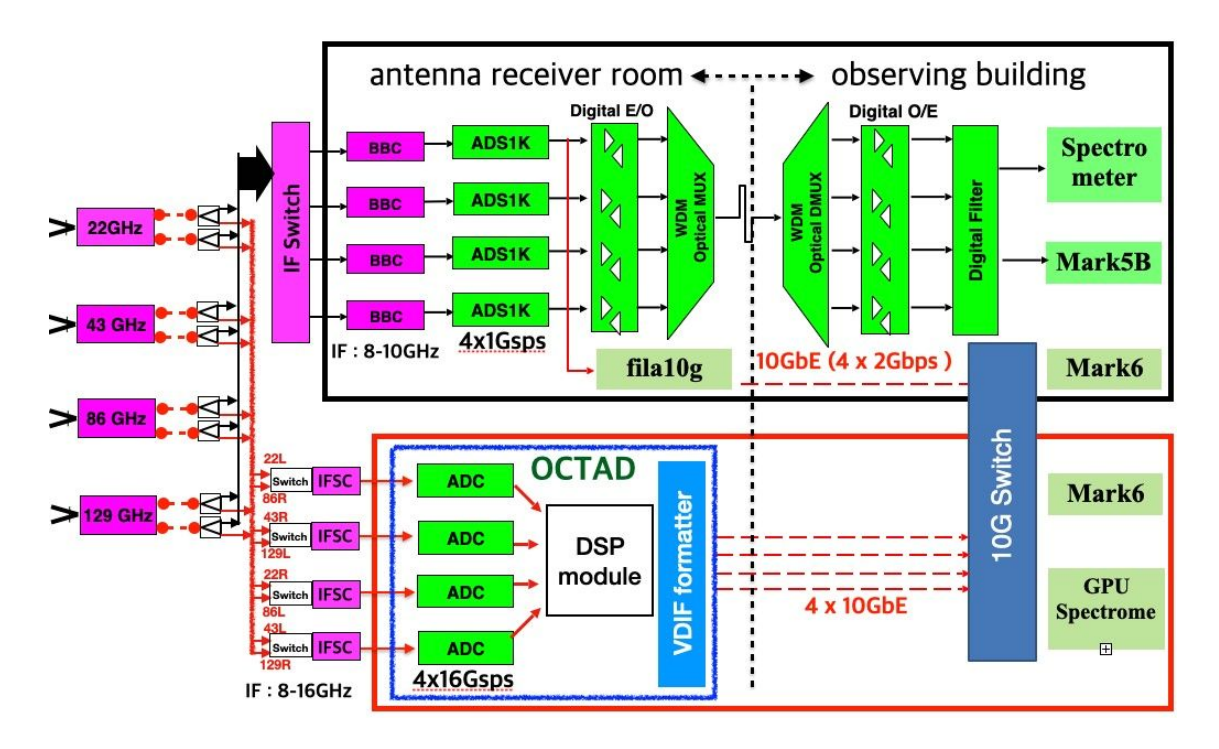


Figure 8: KVN signal flows including a new wide-band sampler OCTAD (from 2020).

Band	Frequency range	IF range
	(GHz)	(GHz)
K	18.0 - 26.0	8.192 - 16.384
Q	$35.0 - 42.0 \; (Low)$	8.192 - 16.384
	$42.0 - 50.0 \; (\mathrm{High})$	
W	85.0 - 100.0  (Low)	8.192 - 16.384
	$100.0-116.0~({ m High})$	
D	125.0 - 142.0	8.0 - 10.0

Table 8: Frequency range of the KVN receiver

# 2.3.4 Receiver noise temperature

Table 9 shows the typical noise temperature of each band. Since the calibration chopper is located before the quasi-optics, the loss of quasi-optics contributes to receiver noise temperature instead of degrading antenna aperture efficiency. Therefore, the noise temperatures of Table 9 include the contribution due to the quasi-optics losses.

The receiver noise temperatures of the three stations are similar to each other except Q-band. Note that the noise temperature of the KUS Q-band receiver is lower than the other stations. This is mainly due to the different type of the thermal isolator of the KUS, which is used to reduce heat flow from the feed horn in the room temperature stage to the cryogenic cooled stage more effectively.

Table 9: KVN receiver noise temperature

Bnad	$T_{ m rx}$
	(K)
K	30 - 40
Q	70 - 80 (40 - 50  for KUS)
W	80 - 100
D	50 - 80

### 2.3.5 System temperatures with wide-band frequencies

A new backend (OCTAD) and the GPU spectrometer have been integrated into the KVN, enabling wide-band observations. Accordingly, we measured the system temperatures in the frequency ranges of the K/Q/W wide-bands, and the results are shown in Table 10 and Figures 9 to 11. The temperature and humidity on 3 November 2021 measured for the K-and the W-low band were  $3.5\,^{\circ}$ C and  $57\,^{\circ}$ K, respectively; on 20 January 2022 measured for the Q band,  $-2.7\,^{\circ}$ C and  $50\,^{\circ}$ K; and on 8 February 2022 measured for the W-high band,  $6.6\,^{\circ}$ C and  $27\,^{\circ}$ K, respectively.

D band measurements were excluded since the receiver does not support wide D band mode (IF range of  $8-10\,\mathrm{GHz}$ ).

Table 10: System temperatures  $(T_{\text{sys}})$  with wide-band frequencies

Band	Freq. range	$T_{\rm sys}$	El.	Date	Site
	(GHz)(K)	(degree)			
$\overline{\mathrm{K}(\mathrm{L})}$	18.0 - 26.0	80 - 120	31 - 54	Nov. 03 2021	KYS
K(R)	18.0 - 26.0	60 - 150	31 - 54	Nov. 03 2021	KYS
Q(L)	35.0 - 50.0	60 - 190	44 - 47	Jan. 20 2022	KYS
Q(R)	35.0 - 50.0	80 - 290	44 - 47	Jan. 20 2022	KYS
W-low $(L)$	85.0 - 100.0	150 - 230	31 - 60	Nov. 03 2021	KYS
W-low $(R)$	85.0 - 100.0	140 - 200	31 - 60	Nov. 03 2021	KYS
W-high $(L)$	100.0 - 116.0	120 - 440	40 - 43	Feb. 08 2022	KUS
W-high $(R)$	100.0 - 116.0	130 - 460	40 - 43	Feb. 08 2022	KUS

# 2.4 Digital Process

### 2.4.1 Digital filter mode

The digital filter bank (DFB) is configurable to various modes according to the required number of streams and bandwidths. The DFB enables us to select in frequency domain 16 data streams of 16 MHz bandwidth from 4 streams of 512 MHz bandwidth. The corresponding data rate of the  $16 \times 16$  MHz stream is 1024 Mbps, which corresponds to the maximum input data rate of the Mark5b recorder. Combining more than one stream, the DFB can produce streams with wider bandwidth such as  $8 \times 32$  MHz,  $4 \times 64$  MHz,  $2 \times 128$  MHz, and  $1 \times 256$  MHz (see Table 11).

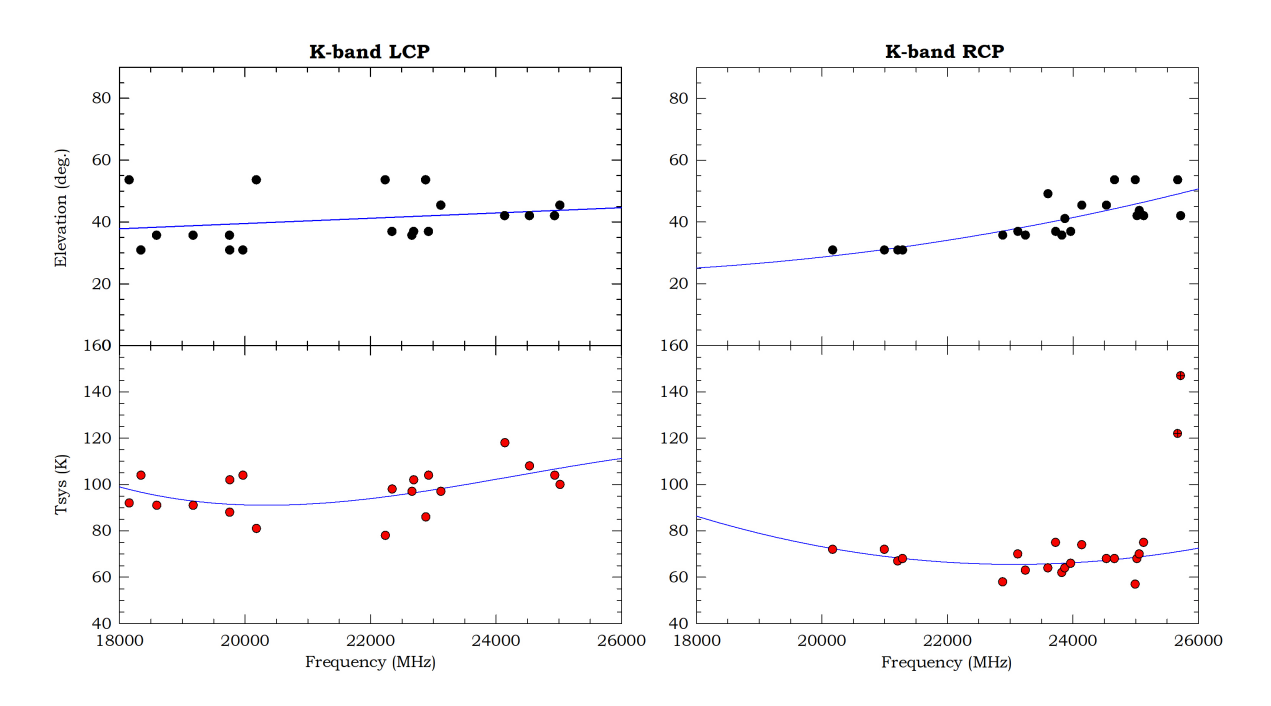


Figure 9: System temperature changes with wide K band frequencies

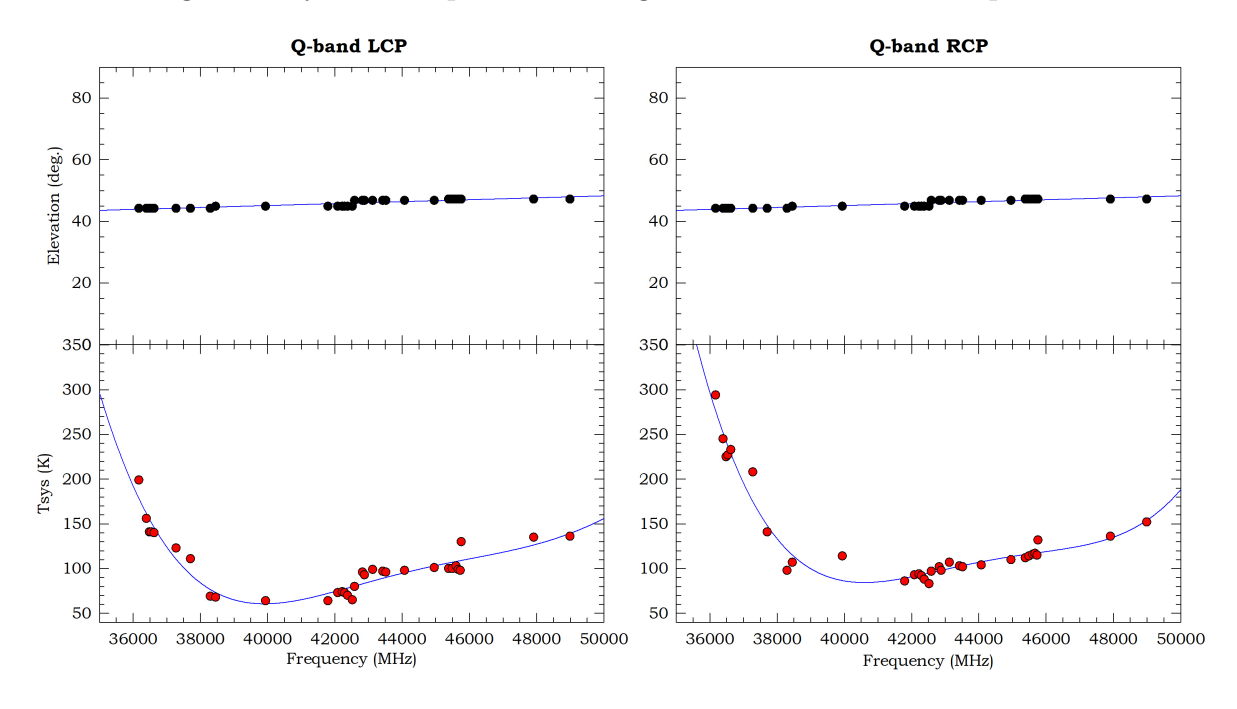


Figure 10: System temperature changes with wide Q band frequencies

A center frequency of a data stream is given by  $BW \cdot (0.5 + N)$ , where BW and N represent a bandwidth of data stream and integer number, respectively. If N is an even number, the data stream is the upper sideband. Otherwise, the data stream is in the lower sideband. Therefore, adjacent data streams have opposite sidebands. The center frequency cannot exceed 512 MHz.

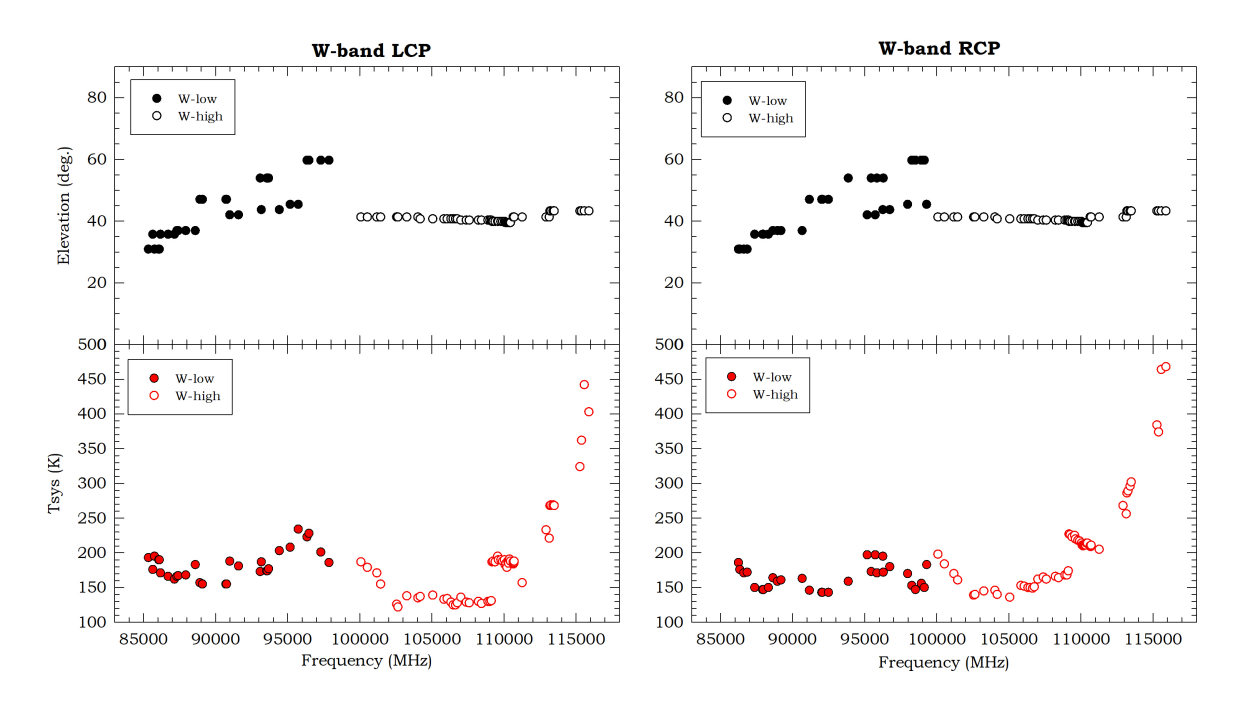


Figure 11: System temperature changes with wide W band frequencies

Table 11: KVN digital filter mode

Bandwidth	Number of streams
(MHz)	
16	16
32	8
64	4
128	2
256	1

#### 2.4.2 Signal processing mode of OCTAD

The OCTAD give various configurable modes. It enables us to select in frequency domain a maximum of 16 data streams from 4 streams of 8192 MHz bandwidth. The maximum output rate is 32 Gbps  $(4 \times 8 \text{ Gbps})$  of which net bandwidth is 8 GHz  $(4 \times 2 \text{ GHz})$  bandwidth). The possible mode of OCTAD is listed in Table 12. There is no restriction on the frequency step and the order of sideband in the OCTAD digital down-converter, unlike the digital filter.

#### 2.4.3 Recorders

KVN station has two recording systems, Mark5b and Mark6.

Mark5b and Mark6 are hard disk recording systems developed at Haystack Observatory, USA. The maximum data rate of Mark5b and Mark6 systems is 1 Gbps and 16 Gbps, respectively. For more details, please see https://www.haystack.mit.edu/haystack-memo-series/mark-5-memos/ and https://www.haystack.mit.edu/haystack-memo-series/mark-6-memos/. At KVN stations, the Mark5b records the output data stream of a digital filter. Refer to sec-

Table 12: KVN OCTAD mode

Bandwidth	Max. Number of streams	Total data rate
(MHz)		(Gbps)
16	16	1
32	16	2
64	16	4
128	16	8
256	16	16
512	16	32
1024	8	32
2048	4	32

tion 2.3.2 for data stream connection and section 2.4.1 for available bandwidth and number of channels of 1 Gbps data stream.

Mark6 records output data streams of four samplers via Fila10G. The Fila10G converts four VSI streams from four samplers into VDIF (VLBI Data Interchange Format) data and sends them to the Mark6 on a 10 GbE network connection. There is no digital filtering function in the Fila10G. Therefore, single IF of Mark6 data of the KVN always has 512 MHz bandwidth. 2 Gbps (1 IF × 512 MHz), 4 Gbps (2 IF × 512 MHz) and 8 Gbps (4 IF × 512 MHz) modes are available in the KVN using the Mark6. The OCTAD VDIF output can be recorded by Mark6. For OCTAD 32 Gbps mode, all two Mark6 should be employed only for the OCTAD output. We cannot record Fila10G output. Therefore, we can observe only no more than four IF signals among eight in OCTAD 32 Gbps mode.

#### 2.4.4 Spectrometers for Single-dish observation

#### • Digital spectrometer

We use an FX-type digital spectrometer (DSM) to process VSI output data from the digital filter of which the aggregation rate is  $1024\,\mathrm{MHz}$  ( $256\,\mathrm{MHz}$  bandwidth). In addition, the DSM can process 4 VSI streams coming from samplers via optical transmission. It processes  $4\times512\,\mathrm{MHz}$  bandwidth data. It can produce both auto- and cross-power spectrum data. The cross-power spectrum data are used for polarization observation. The available number of FFT points is fixed to 4096 per stream in all modes.

### • GPU Spectrometer

The GPU (Graphics Processing Unit) spectrometer receives VDIF data streams from OCTAD and makes FFT calculations to produce power spectrum. Depending on the performance of GPU cards and the host server of the GPU spectrometer in each station, available modes are different. They are summarized in Tables 13 and 14. The GPU spectrometer can support various numbers of FFT points thanks to its high flexibility. We can get at least 4096 FFT points in a 32 MHz stream. The GPU spectrometer can produce not only auto- but also cross-power spectrum data as the digital spectrometer does. However, polarization observation mode using the cross-power spectrum output

Table 13: Available mode of the GPU spectrometer at KTN and KUS

Bandwidth	Number of streams	Total data rate
(MHz)		(Gbps)
32	16	2
64	4	1
128	2	1

Table 14: Available mode of the GPU spectrometer at KYS

Bandwidth	Number of streams	Total data rate
(MHz)		(Gbps)
32	16	2
64	16	4
128	16	8
256	8	8
512	4	8
1024	2	8
2048	1	8

of the GPU spectrometer is not available yet because it is under test.

#### 2.4.5 Correlator

#### • Correlators in KJCC

The KJCC(Korea-Japan correlation Center) gathers the raw VLBI observation data from each site of KVN, VERA/JVN, and CVN, and performs the correlation process with two VLBI correlators.

The first one, Daejeon Correlator, is one of the fastest VLBI correlators in the world and is used for processing the KaVA and EAVN observations mainly. It is capable to correlate the data streams of max. 8 Gbps for max. 16 stations in one pass, to produce the correlated output of 8192 spectral points for each sub-bands. The number of spectral points is reduced to 128 for continuum, 512 for line observation after the correlation process by channel integration.

The second one, DiFX (Distributed FX), is the world-famous software correlator and is used for processing the KVN observations. It provides quite flexible correlation modes. You can request the accumulation time and the frequency resolution appropriate for your science purpose.

For the final correlation output, the default accumulation time is 1.6384 seconds for the Daejeon correlator or 0.8192 seconds for DiFX correlator. The final frequency resolutions are  $16\,\mathrm{MHz}/128$  for continuum observations, and  $16\,\mathrm{MHz}/512$  for line observations in default.

# • Correlation mode and integration time

The KJCC is currently able to support the following correlation modes (see Table 15).

Table 15: Correlation mode of the KJCC

Obs.	Total	Bandwidth	# of	Minimum	# of Freq. Channels
Mode	Data Rate	/sub-band	sub-bands	Accum. Time	/sub-band
$\overline{\mathrm{C5}}$	$1024\mathrm{Mbps}$	$16\mathrm{MHz}$	16	$1.6384 \; { m sec}$	8192
C4	$1024\mathrm{Mbps}$	$32\mathrm{MHz}$	8	$0.8192  \sec$	8192
C3	$1024\mathrm{Mbps}$	$64\mathrm{MHz}$	4	$0.4096  \sec$	8192
C2	$1024\mathrm{Mbps}$	$128\mathrm{MHz}$	2	$0.2048  \sec$	8192
C1	$1024\mathrm{Mbps}$	$256\mathrm{MHz}$	1	$0.1024~{ m sec}$	8192
W1	$2048\mathrm{Mbps}$	$512\mathrm{MHz}$	1	$0.0512~{ m sec}$	8192
W2	$4096\mathrm{Mbps}$	$512\mathrm{MHz}$	2	$0.0512~{ m sec}$	8192
W4	$8192\mathrm{Mbps}$	$512\mathrm{MHz}$	4	$0.0512~{ m sec}$	8192

#### • CODA and FITS

The KJCC supports the following number of frequency channels for preparing FITS file.

- Basic output channel of correlator: 8192 frequency channel
- Continuum: 128 frequency channel (64 channels integrated in post-correlation)
- Spectral line: 512 frequency channel (16 channels integrated in post-correlation)

#### • FITS delivery

Correlations will be done using either the DiFX or the Daejeon correlator. The KJCC will deliver the FITS file to PI by using an FTP server or mobile disk.

- When correlation is finished, the FITS file will be prepared through post-processing, and then the KJCC will announce the correlation processing completion to PI by e-mail. In the e-mail, PI will be able to get the FITS file by temporary URL link.
- The PI should download the FITS file as soon as possible, and check the FITS file using his/her preferred analysis tool. And then the PI should give his response to KJCC with "Success" (data quality is good) or "Fail" (download fail, bad FITS file or data quality is bad, etc). Especially in the case of the "Fail" opinion, please send the error message to the KJCC, then your quick response for the FITS will be helpful for the KJCC to solve the problem as soon as possible.
- The KJCC would like to receive PI's response within 2 weeks after announcing the e-mail. If there is no response within 4 weeks, the KJCC determines that PI is regarded as his response as "Success".
- In case of "Fail", according to the fail type, the KJCC will conduct the URL check, file reconstruction, or re-correlation, and then an announcement will be sent again to PI via e-mail.

- In case of "Success", correlation processing for that observation will be closed (at that time, download link in temporary URL will be unavailable), and the tapes or disk module will be included to release pool for recycling.
- The FITS file provided to PI will be stored at the observation data archive separately. PI SHOULD analyze, perform the research, and publish the paper within some period(in general, 18 months). After 18 months, the FITS file stored in the archive system will be opened to the public who need to do his/her research using that FITS according to the procedures.

### Archiving policy

The KJCC organizes the archiving policy for observation data, CODA, and FITS file as below.

- Observation data: 2 weeks after FITS release (usually, about 2 months after observation), and then it will be released.
- CODA: if correlated data is used for astrometry or geodesy, it is permanently stored at the CODA server. Otherwise, the correlated raw data and CODA file system will be deleted after receiving the response from PI.
- FITS: it is permanently archived at the Archiving server.

### • Expected time of correlation

Correlation processing will be about 1 week for preparing 1st version of FITS, after the data arrival of the last station. However, the KJCC team will do their best to make correlation results as fast as possible to deliver the FITS file to PI.

# 2.5 Calibration

#### 2.5.1 Amplitude calibration

System temperatures in Kelvin ( $T_{\rm sys}$ ) are measured during observations at KVN stations once every user-specified interval (default 10 sec) to calibrate amplitude variation in time due mainly to atmospheric fluctuation. The measured  $T_{\rm sys}$  is a sum of three temperatures: the receiver temperature, the spillover temperature, and the contribution of the atmosphere as described in Petrov et al. (2012) [4]. These  $T_{\rm sys}$  values can be converted to SEFD (System Equivalent Flux Density) by dividing by the KVN antenna gains in K/Jy. The elevation dependence of the antenna gains are also corrected based on the normalized gain curves with lease-squared-fitted second-order polynomials as derived in Lee et al. (2011) [5].

Additional amplitude correction for the atmospheric opacity above an antenna is performed by conducting a sky tipping curve analysis according to the method described in Mangum (2000). In practice, the system temperatures  $(T_{\text{sys}}^*)$  corrected for the atmospheric opacity are estimated based on the sky tipping curve measurements once every user-specified interval (default before and after an experiment). Further corrections are made to the KVN observations taken with 2-bit (4-level) sampling, for the systematic effects of the non-optimal setting of the quantizer voltage thresholds.

The amplitude calibrations with the KVN are accurate to 15% or better at 22 and 43 GHz. However, it is recommended to observe a few amplitude calibrators during the

scheduled observation time, allowing for (a) the assessment of the relative gains of KVN antennas and gain differences between IF-bands at each station, and (b) the confirmation of the correlation coefficient correction assuming that you have contemporaneous source flux densities obtained with other VLBI networks independent of the KVN observations.

# 2.6 KVN geodetic VLBI measurement

Obtaining accurate antenna positions is important in the VLBI system, especially for high precision astrometry. KVN antenna positions are regularly monitored using GPS and geodetic VLBI observations. The K-band geodesy VLBI program between KVN and VERA has been started in 2011. Current KVN antenna positions (see Figure 12) are obtained from the KaVA K-band geodesy on 2014 January 24. The typical 1-sigma errors of geodetic solutions are about 0.4 cm in X, Y, and Z directions. Based on 22-epoch KaVA K-band geodetic observations from September 2012 to December 2016, uncertainties of KVN antenna positions are  $\sim 2.38$  cm at KYS,  $\sim 2.55$  cm at KUS and  $\sim 1.58$  cm at KTN.

The KVN antenna positions are described in the section 2.1.3.

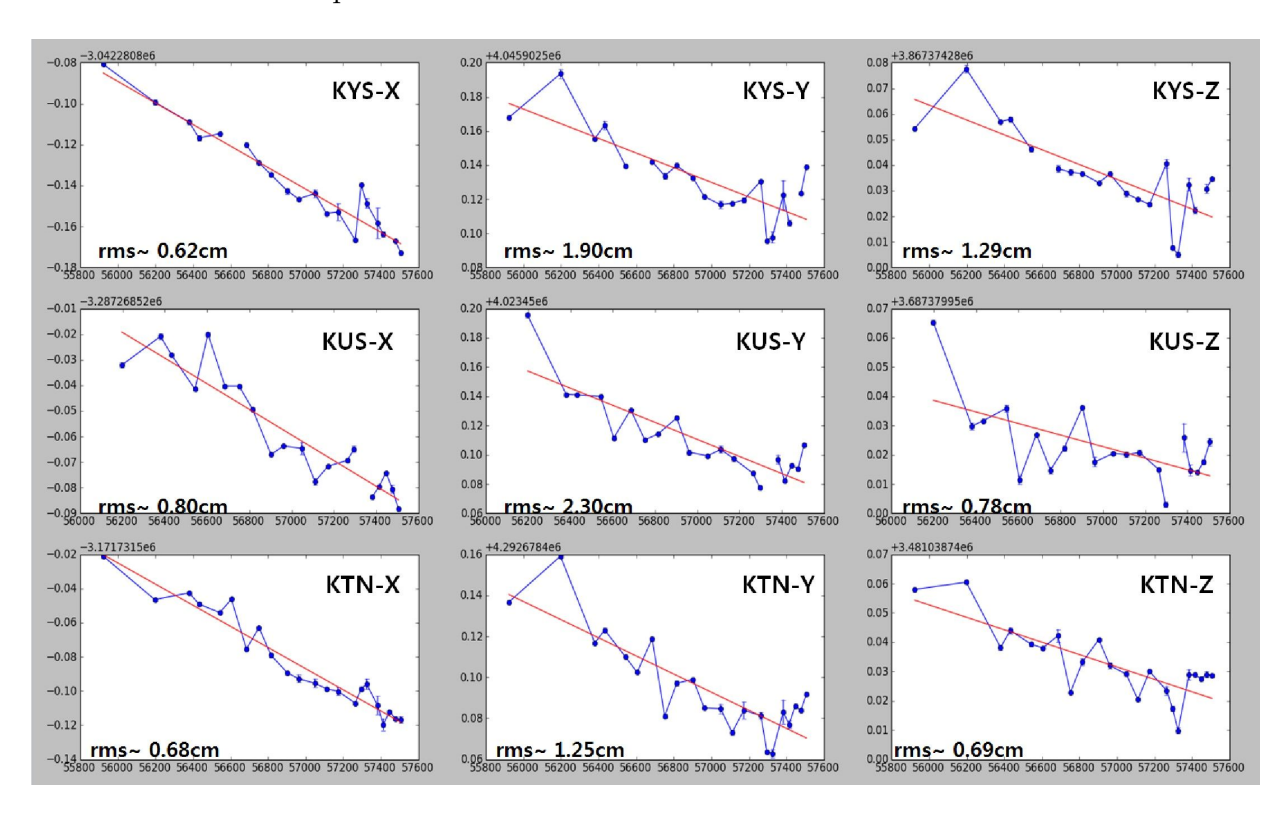


Figure 12: The trend of KVN antenna positions (IVP) in ITRF2014 coordinate system. The x and y axes are MJD and X/Y/Z in meter. The linear fitted is applied to the measurements, shown as red line, and its deviation is also presented in each axis as "rms".

# 3 Observing proposal

# 3.1 Observing mode

### 3.1.1 Multi-frequency observation

Simultaneous multi-frequency observation is a unique capability of the KVN with which we can calibrate out the short-term phase fluctuations at higher frequency data by referencing the phase solution obtained from lower frequency data. This phase referencing technique allows us to integrate the data for the time scale much longer than the coherent time scale of atmospheric phase fluctuation and so to observe weak sources at mm-wavelength efficiently. For multi-frequency observations, we can select no more than 4 IFs among 8 IF signals (= 4 receivers × 2 polarizations).

### 3.1.2 Fast position switching observation

The slewing speed and acceleration rate of the KVN antenna are 3 °/sec and 3 °/sec<sup>2</sup>, respectively. Due to this high speed and acceleration rate, the KVN antenna can switch its pointing from target to calibrator in a short period.

### 3.1.3 2 Gbps/4 Gbps/8 Gbps observation modes (NEW!)

 $2 \,\mathrm{Gbps} \ (1 \times 512 \,\mathrm{MHz}), \ 4 \,\mathrm{Gbps} \ (2 \times 512 \,\mathrm{MHz}), \ 8 \,\mathrm{Gbps} \ (4 \times 512 \,\mathrm{MHz}) \ \mathrm{modes}, \ \mathrm{which} \ \mathrm{use}$  fila  $10 \,\mathrm{G}$  and Mark 6 recorder, have been fully evaluated in 2017. These modes are available for common use observations from the  $2017 \,\mathrm{B}$  semester. For multi-frequency observations, we can select  $1, 2, \mathrm{or} \ 4 \,\mathrm{IFs} \ \mathrm{among} \ 8 \,\mathrm{IF} \ \mathrm{signals} \ (= 4 \,\mathrm{receivers} \times 2 \,\mathrm{polarizations}).$  Note that it is not allowed to assign multiple  $512 \,\mathrm{MHz} \ \mathrm{streams}$  for one IF.

# 3.2 Angular resolution

Table 16 shows the maximum lengths (B) of the KVN baselines in km and the corresponding resolutions ( $\theta_{HPBW}$ ) in milli-arcsecond (mas), which is estimated as  $\theta_{HPBW}$  (mas)  $\sim 20627 \cdot \lambda(\text{mm})/\text{B(km)}$ .

Table 16: Angular	resolutions a	t each KVN	baseline and	frequency
-------------------	---------------	------------	--------------	-----------

Baseline	B (km)	$\theta$	$\theta_{\mathrm{HPBW}} \; (\mathrm{mas})$		
		K	Q	W	D
KYS-KUS	305	9.2	4.7	2.4	1.6
KUS-KTN	358	7.9	4.0	2.0	1.3
KTN-KYS	476	5.9	3.0	1.5	1.0

# 3.3 Baseline sensitivity

Table 17 shows sensitivities of the KVN baselines as follow: (1) frequency band, (2) nominal frequency range of KVN receivers, (3) system temperature, (4) typical KVN system-

equivalent-flux-density at zenith, (5) antenna gain at the optimal elevation, (6) typical KVN baseline sensitivity for the aggregated recorded data rate of 1024 Mbps, the integration time of 100 sec (K-band), 60 sec (Q-band), and 30 sec (W/D-band), and the bandwidth of 256 MHz, and (7) typical KVN 3-baseline image sensitivity for the on-source integration time of 8 hr.

Table 17: Baseline sensitivity of the KVN

Freq. band	Freq. range	$T_{\rm sys}$	SEFD	Gain	$\Delta S$	$\Delta I$
	(GHz)	(K)	(Jy)	(K/Jy)	(mJy)	(mJy/beam)
(1)	(2)	(3)	(4)	(5)	(6)	(7)
K	21.25 - 23.25	100	1288	0.078	12	0.2
Q	43.11 – 44.11	150	1919	0.078	18	0.3
W	85 – 95	200	3214	0.062	29	0.6
D	125 – 142	250	5952	0.043	54	1.0

# 3.4 System temperature

Figure 13 shows seasonal variation of system temperature at each KVN site. The zenith system temperatures corrected for atmospheric attenuation at K-, Q-, W-, and D-bands are presented by four panels from top to bottom, respectively.

### 3.5 Astrometric observation

For accurate astrometric observations, many items (antenna positions, calibrators, schedule, etc.) should be carefully considered and prepared. At present, astrometric VLBI observations with the KVN are not supported. However, we started AGN/Maser astrometric test observations to check the feasibility and those results will be reported next year. If you want to make an astrometric observation, please contact us.

# 4 Observation and Data Reduction

# 4.1 Preparation of observation and correlation

#### 4.1.1 General information

For the accepted proposals, the users have to prepare the observing schedule file before the observation. The observer who is not familiar with the KVN system is recommended to consult contact persons of the KVN group to prepare schedules, especially for some observations such as phase referencing, polarimetry, and/or spectral line, etc. The detailed information about observation planning and scheduling can be downloaded from the KVN homepage<sup>2</sup>.

<sup>&</sup>lt;sup>2</sup>https://radio.kasi.re.kr/kvn/notice\_user.php

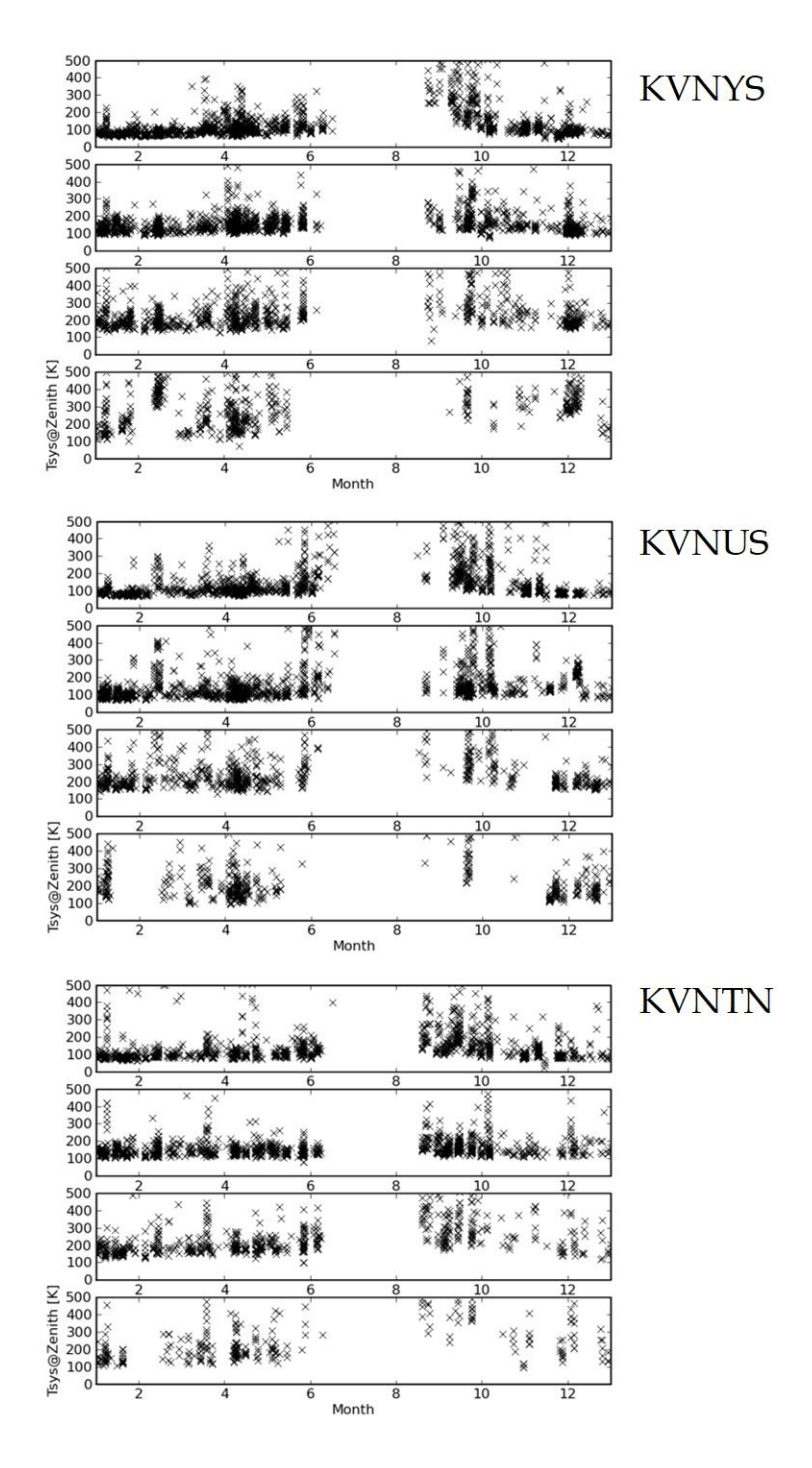


Figure 13: System temperatures of each KVN telescope

# 4.1.2 Observation

All KVN experiments should be scheduled using the VEX (VLBI experiment) file. You can either edit and modify the KVN VEX example files or use the VLBA scheduling program

SCHED<sup>3</sup>. It is recommended to use SCHED for your scheduling because SCHED provides useful information and many aspects of planning VLBI observations and you can also avoid many mistakes arising from editing the VEX manually. The user needs to submit the VEX or key files two weeks before the observation. KVN AOC staff will check your schedule and proceed with the observations.

#### 4.1.3 Correlation

After the observation, the correlation process will be carried out by the Daejeon correlator or DiFX correlator according to the requested parameters. The user is asked to examine the correlated data and to report whether the correlation was properly done so that the disk modules and storage used for observation can be released and recycled, or re-correlation is needed if there is some problem. In principle, the disk modules (raw data) used for observations will be recycled two months later after the correlation. For more information, please refer to the correlation status report.

### 4.2 Data reduction

#### 4.2.1 VLBI data reduction with AIPS

Here we introduce a very brief way of reducing VLBI data with KVN (or EAVN). For more detail, please have a look at the data reduction manual<sup>4</sup>. Figure 14 shows one of the procedures of reducing the KVN (or EAVN) observations.

### 4.3 Correlator status

### 4.3.1 Daejeon Correlator

Figure 15 shows the conceptual block diagram of the Daejeon Correlator. Several VLBI data playbacks will be used in our combined VLBI networks, such as Mark5B, VERA2000, OCTADISK, and optical fiber which shall be connected in near future. Some of them have the VSI-H compatible interface, while the others take a different interface for the data transmission. In addition, they have also their maximum data recording/playing back rates respectively. To absorb all of these differences and inhomogeneity among these existing VLBI data playback systems, the Raw VLBI Data Buffer (RVDB) was introduced, which is a big data server with many large RAID disks and several kinds of VLBI data interfaces. The VLBI Correlation Subsystem (VCS) shall receive the VLBI data from the RVDB system, shall calculate the correlation between every possible pair of data inputs with proper control parameters given from the monitor and control operation computer, and they shall dump the correlation results into the data archive system. A data archive system is also a kind of data server, which is used to capture the correlated data output from the VCS and to save them as a structured file system. Finally, there is also the correlator control and operation software for the overall system.

<sup>3</sup>http://www.aoc.nrao.edu/~cwalker/sched/sched.html

<sup>4</sup>https://radio.kasi.re.kr/kvn/data\_reduction.php

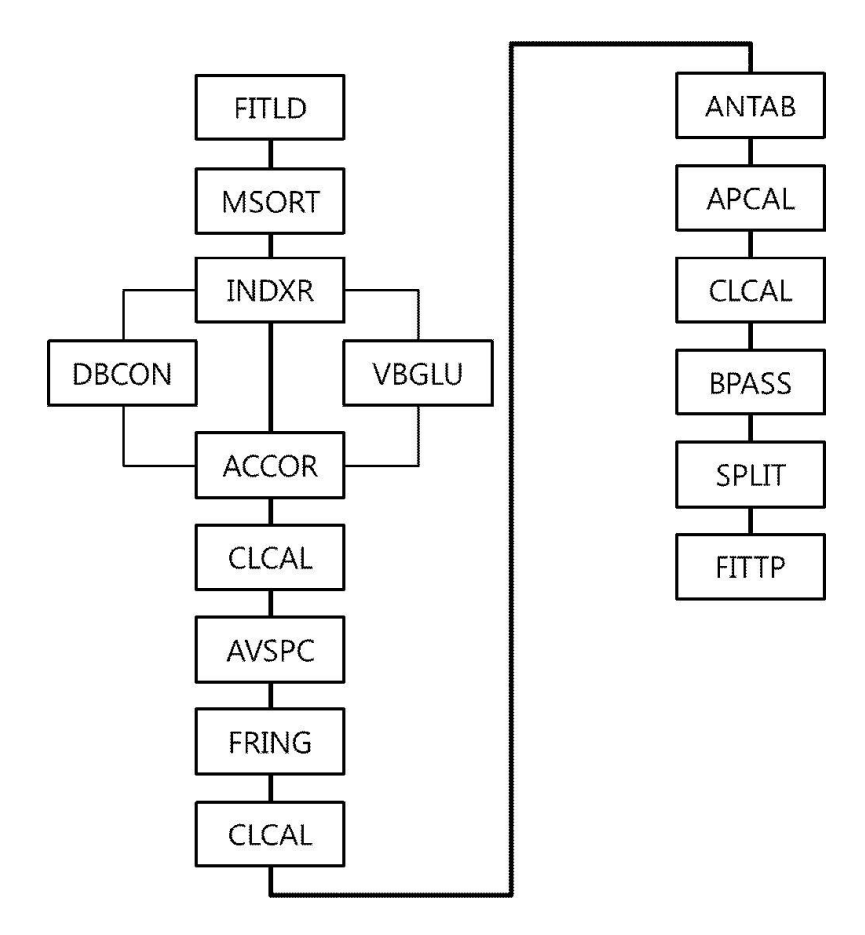


Figure 14: Data reduction flow chart with AIPS

Playback system KVN is now using the Mark5B system for recording and playback the observed data. KASI participated in Mark5B development with Haystack Observatory as a member of an international consortium. It can support the VSI compatible and RAID-based HDD storage system. Recording and playing back speed is 1024 Mbps. DIR2000 is widely used in VERA for recording and playback with 1024 Mbps. Recently the manufacturer of DIR2000 had been stopped to manufacture, so NAOJ developed a new playing back system named VERA2000, which is modified by the DIR1000H system for only supporting playing back. For improving observation and correlation efficiency, VERA uses the OCTADISK system for KaVA observations from 2014. So Daejeon Correlator also adopted the OCTADISK system, which has the same functions of OCTADDB installed in RVDB (Refer the next paragraph).

RVDB system RVDB system, which is developed by NAOJ, consists of Data Input-Output (DIO) (currently named OCTAVIA), 10 GbE switch, and Disk Data Buffer (DDB) (currently named OCTADDB). It can record the data with a maximum of 2048 Mbps, and can playback the observed data to the correlator with nominal 2048 Mbps. So, it has a function such as a 2048 Mbps recorder and playback at the same time. As shown in Figure 15, the different types of playback systems are used in Daejeon Correlator. So, the purpose of the RVDB system is that it can adjust the data format and easily synchronize the data

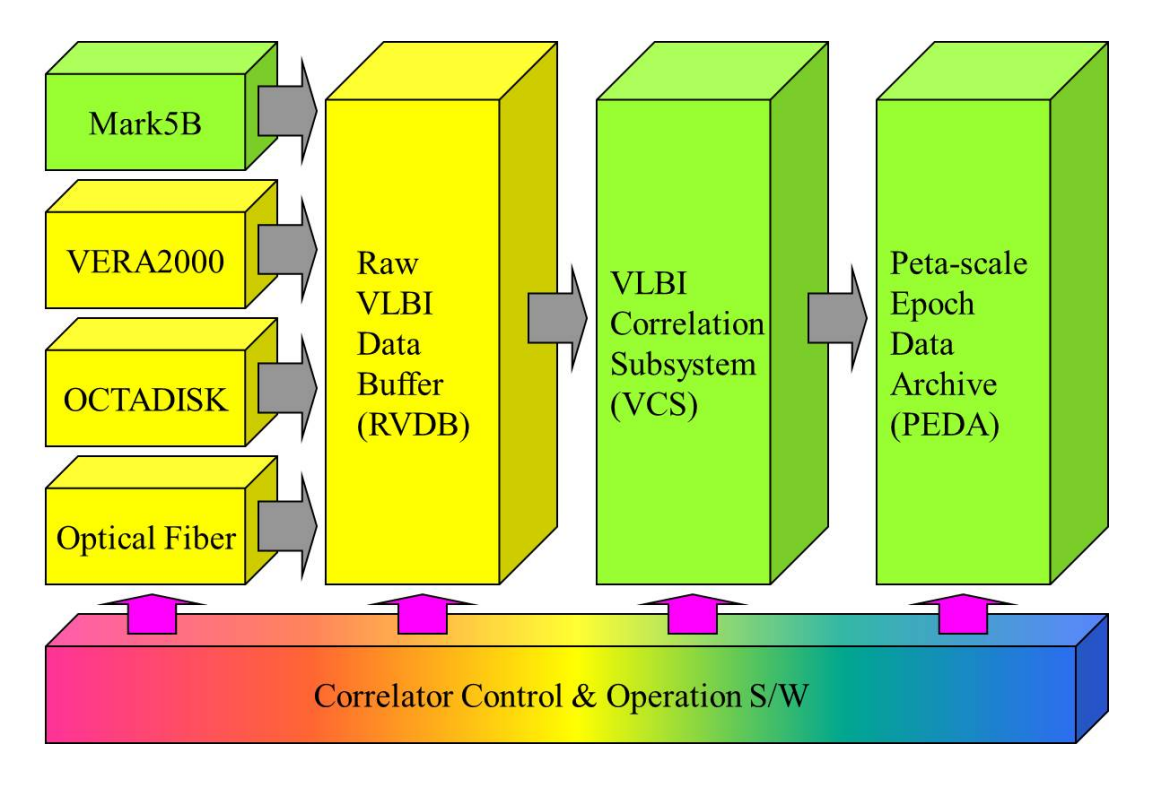


Figure 15: Block diagram of Daejeon Correlator

during playback and maintain the buffering between recorder speed and correlation speed.

VLBI Correlation subsystem — The main specification of VCS is described in Table 18. The VCS can process a total of 120 cross-correlations and 16 auto-correlations intended for a maximum of 16 stations, maximum of 8192 Mbps (4-streams  $\times$  1 Gbps/2-bit/64 MHz clock) input data rates per station. The design architecture for the correlator is FX-based and it will use the variable length of FFT (Fast Fourier Transform) to maintain the 0.05 km/sec resolution of velocity at 22 GHz. The maximum delay is  $\pm$  36,000 km and the maximum fringe tracking is 1.075 kHz. The number of frequency channels per correlation output is 8,192.

Correlated VLBI Data Buffer (CVDB) (old name: Data Archive System) The basic architecture is a CPU cluster connected with Infiniband. For KaVA, the first phase data archive system with about 119 TB capacity has been implemented. It has four 10 Gigabit Ethernet input ports to connect with VCS output and one 10 GbE Ethernet port is connected with the data file system for sharing the disk. We have a plan to increase the system capacity to support the EAVN in near future. CODA file system is used in the data archive system for making the file system from correlated raw data, which is revised with ccCODA 2.0 library used in Mitaka FX correlator with some modification. A new CODA file system based on the ccCODA 2.1 library was installed. Figure 16 shows the view of the Daejeon Correlator installed at Korea-Japan Correlation Center (KJCC) located in KASI, Daejeon, Korea.

Table 18: Specification of Daejeon Correlator

Num. of antennas	16
Num. of inputs/antenna	4 bands $(4F\times1P, 2F\times2P, 1F\times2P + 2F\times1P)$
Max. Num. of corr./input	120  cross + 16  auto
· -	·
Sub-array	$2 \operatorname{case} (12 + 4, 8 + 8)$
Bandwidth	$512\mathrm{MHz}$
Sampling, Digitization	1 Gbps by 2bit/sample
Max. data rate/antenna	2 Gbps VSI-H (32 parallels, 64 MHz clock)
Max. delay compensation	$\pm 36,000  \mathrm{km}$
Max. fringe tracking	$1.075\mathrm{kHz}$
Design architecture	FX-type with FPGA
FFT word length	16 + 16 bits fixed point for real, imaginary
Integration time	$25.6\mathrm{msec}\sim10.24\mathrm{sec}$
Data output channels	8192 channels
Data output rate	Max. 1.4 GB/sec at 25.6 msec integration time

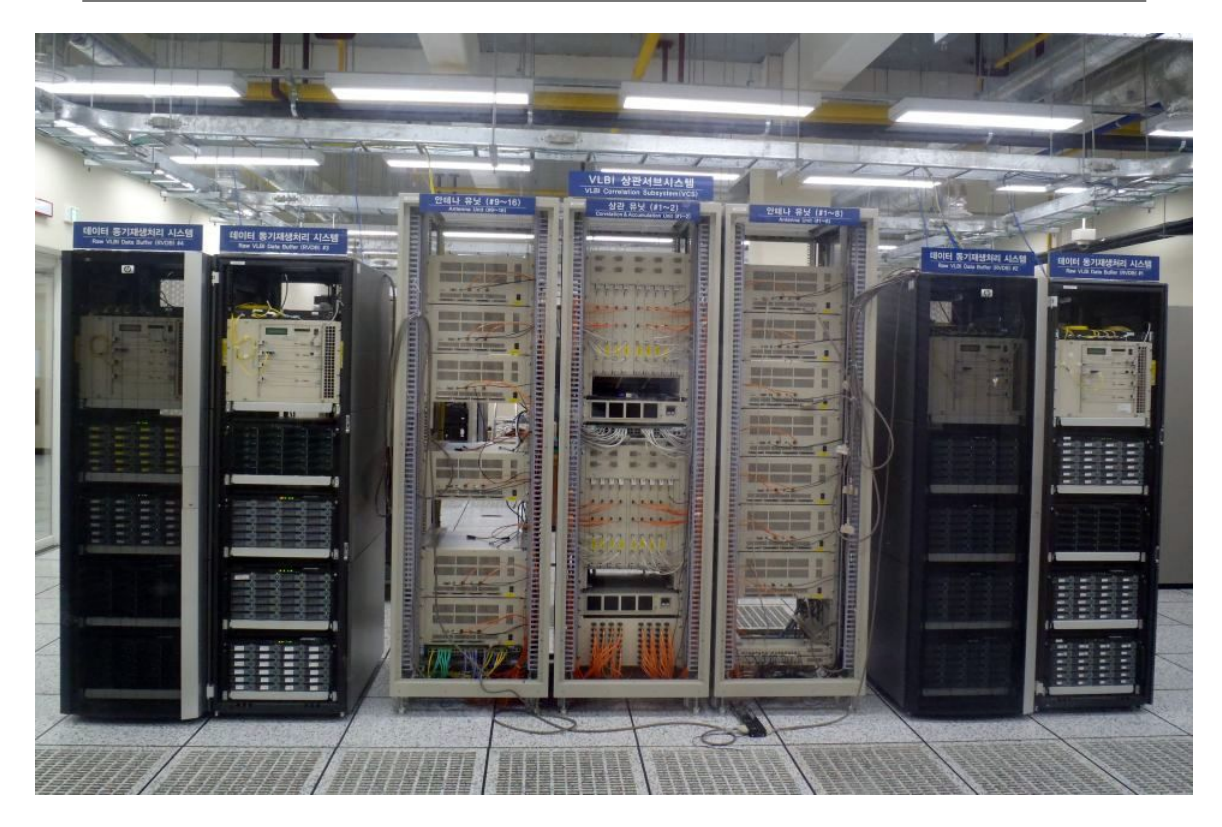


Figure 16: Daejeon Correlator installed at Korea-Japan Correlation Center

# 4.3.2 Correlation Processing

A detailed description of this part is provided in previous Section 2.4.5.

### 4.3.3 Performance of Daejeon Correlator (Continuum/Spectral-line)

Data Analysis (@AIPS) To verify the performance of the Daejeon correlator, data analysis was conducted. For the comparison of correlation results, the Daejeon correlator, Mitaka FX, and DiFX correlator were utilized. Observation experiments were listed in Table 19. We confirmed that the results of the Daejeon Correlator had a consistent and correct value. Here we summarize the results for R11027B and K11017A. The procedure of data analysis was performed as follows. And the same parameter was used for all correlation results during analysis. Analysis for spectral-line was adopted with the following procedure, while analysis for continuum was excluded for 9 and 10 stages.

Experiment	Object	Source	Recorder	Reference
R11027B	Daejeon Correlator	Continuum	DIR2K, Mark5B	MTK FX,
	evaluation	/Spectral line		DiFX
R11026A	Long time phase	Continuum	DIR1K, DIR2K,	MTK FX
	monitoring		Mark5B	
K11017A	2 frequency	Continuum	Mark5B	DiFX
	simultaneous obs.			
K12098C	4 frequency	Continuum	Mark5B	DiFX
	simultaneous obs.			

Table 19: Observation experiments list

# Analysis result for continuum (R11027B)

Spectrum of raw data Figure 17 shows the spectrum shape after completion of FITLD, MSORT, USUBA, and INDXR tasks based on the FITS file generated by the Daejeon Correlator and the DiFX. The target source is 3C 454.3 for continuum with KYS and KUS baseline. Phase for all of 16 IF are continuously changed. The phase slope of the DiFX is lower than that of the Daejeon Correlator. However, we think this is caused by adopting the clock offset precisely while DiFX correlation. After fringe fitting, these values would be deleted and there is no serious problem in the current phase slope.

Gain amplitude We looked into the variation of GAIN for each source during the whole observation time after ACCOR. Then as shown in Figure 18, the gain amplitude was continuously stable for source with long time integration. However, in the case of source with a short integration time, the gain amplitude pattern for the Daejeon Correlator was unstable for the time range (between 22:00 and 03:00 for Sgr A\* and Sgr B2(M)), compared with the DiFX. This phenomenon was only seen in the KVN stations, and is believed to be due to data synchronization while playing back. This phenomenon only occurred beginning of the scan about 2–4 sec., while the other time range is stable. We recommend the continuous recording of Mark5B while observation.

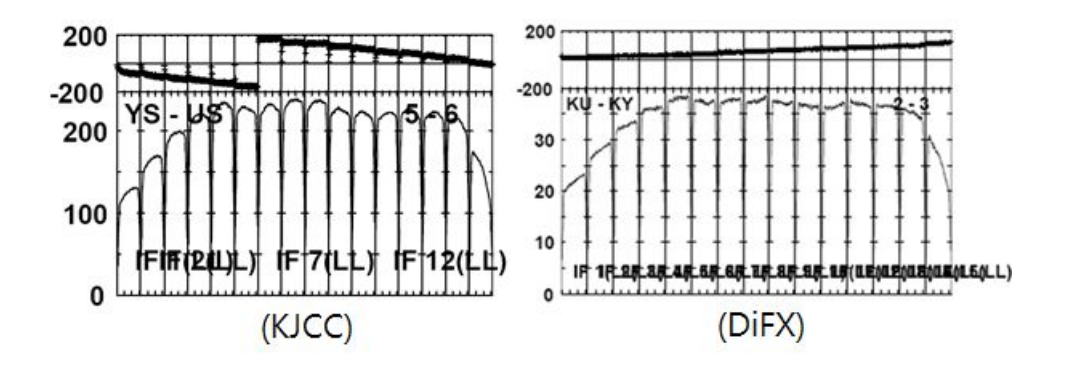


Figure 17: Spectrum shape of 16 IF continuum for KYS-KUS baseline

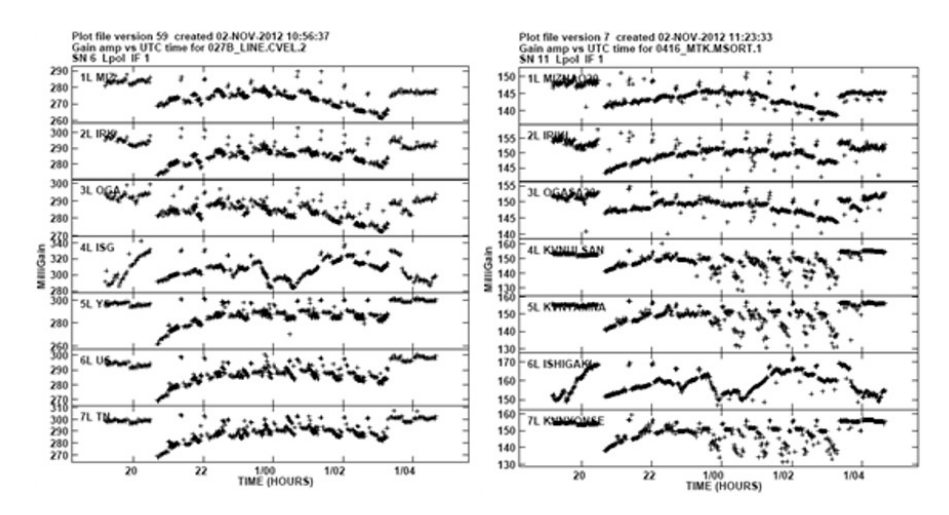


Figure 18: Variation pattern of gain amplitude for all stations with  $9^{th}$  IF. Left (Daejeon Correlator), Right (DiFX).

SNR, Delay, Rate after fringe fitting Figure 19 shows the SNR, Delay, and Rate for each baseline, respectively. The reference was set as the KUS station. Integration time for fringe fitting is 30 sec, and SNR cutoff is 3. 3C 454.3 which is a very strong radio source in continuum sources was used, and the phase pattern was remarkable. For the comparison with DiFX, all of the patterns for each result are almost similar without any problems.

Closure phase Using the previous fringe fitting result, the closure phase for 3C 454.3 was obtained and showed in Figure 20. We confirmed that the closure phase was existed within about 5 degrees by calculating with a variation of phase for whole observation time and by integrating 50–64 channels value of  $1^{st}$  IF for both Daejeon Correlator and DiFX.

**Spectrum shape after fringe fitting** Figure 21 shows the spectrum shape after fringe fitting. We draw again the spectrum to check phase residual by adopting the value of delay, rate after fringe fitting. For a more detailed comparison, the range of phase was enlarged to 10 degrees and 8 IFs were only shown. Phase residual for the spectrum of Daejeon Correlator and DiFX was almost the same with 0 value.

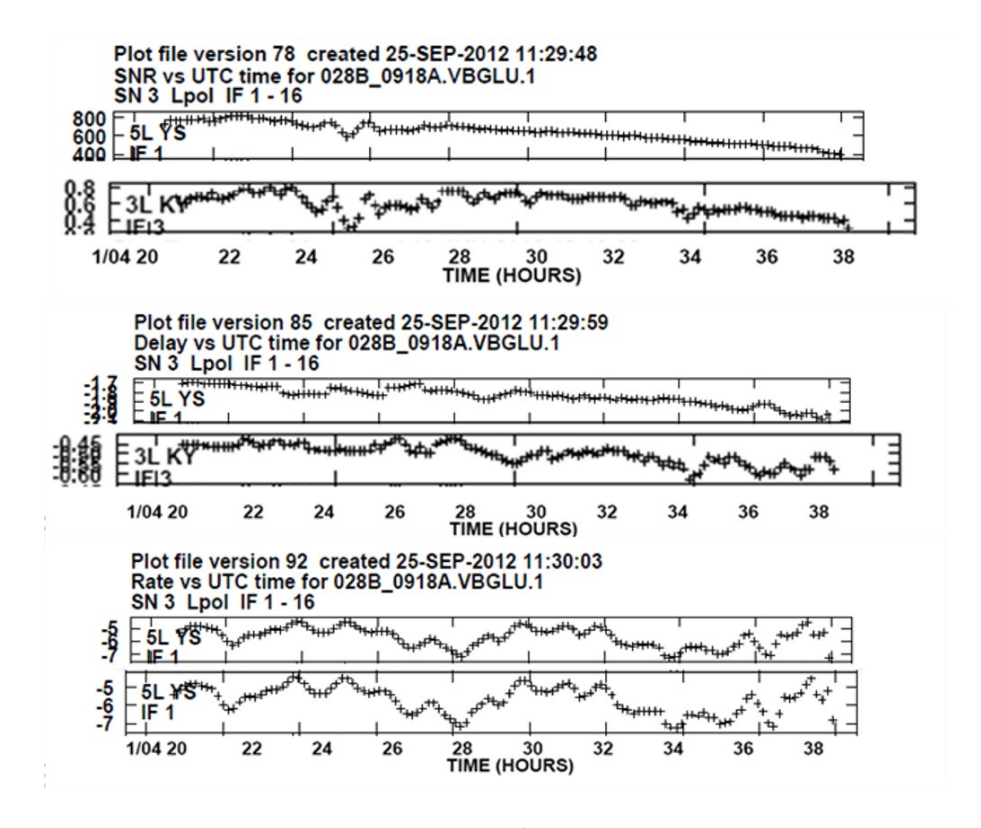


Figure 19: SNR, Delay, Rate after FRING for  $1^{st}$  IF of the KYS. Upper (Daejeon Correlator), Bottom (DiFX).

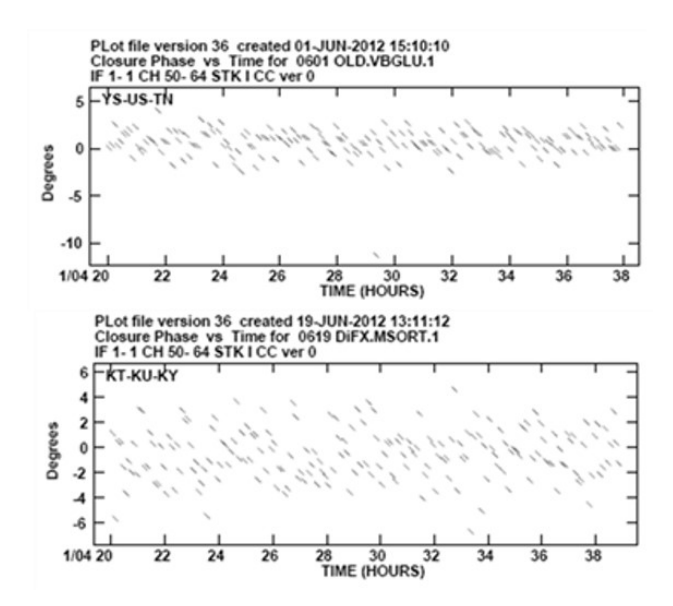


Figure 20: Closure phase after fringe fitting. Upper (Daejeon Correlator), Bottom (DiFX).

**Imaging performance** A new result file was generated by averaging all IFs, all channels, and whole observation time for tables of 3C 454.3 by using the SPLIT task. The 2-dimensional image map was generated using a new result file and is shown in Figure 22. In Figure 22, KVN 3 stations were only used for comparison to DiFX. Flux for Daejeon

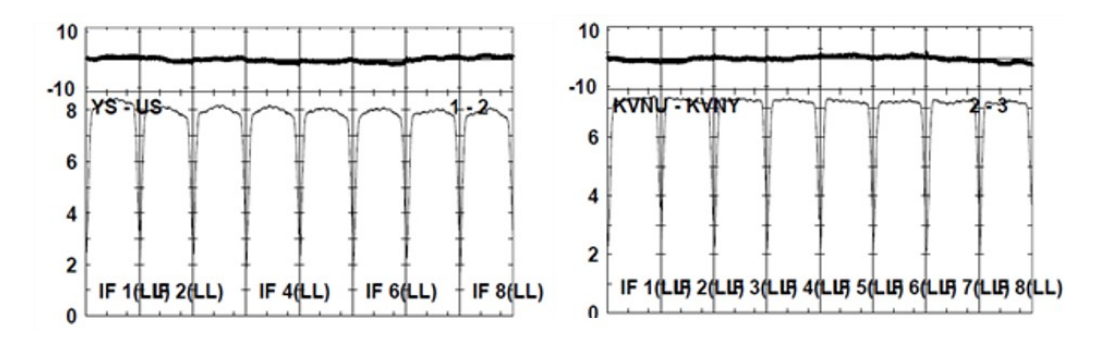


Figure 21: Spectrum shape after fringe fitting. Left (Daejeon Correlator), Right (DiFX).

Correlator is 0.75 Jy/beam, which is less than about 12 %, compared with 0.84 Jy/beam of DiFX, while the dynamic range is almost the same.

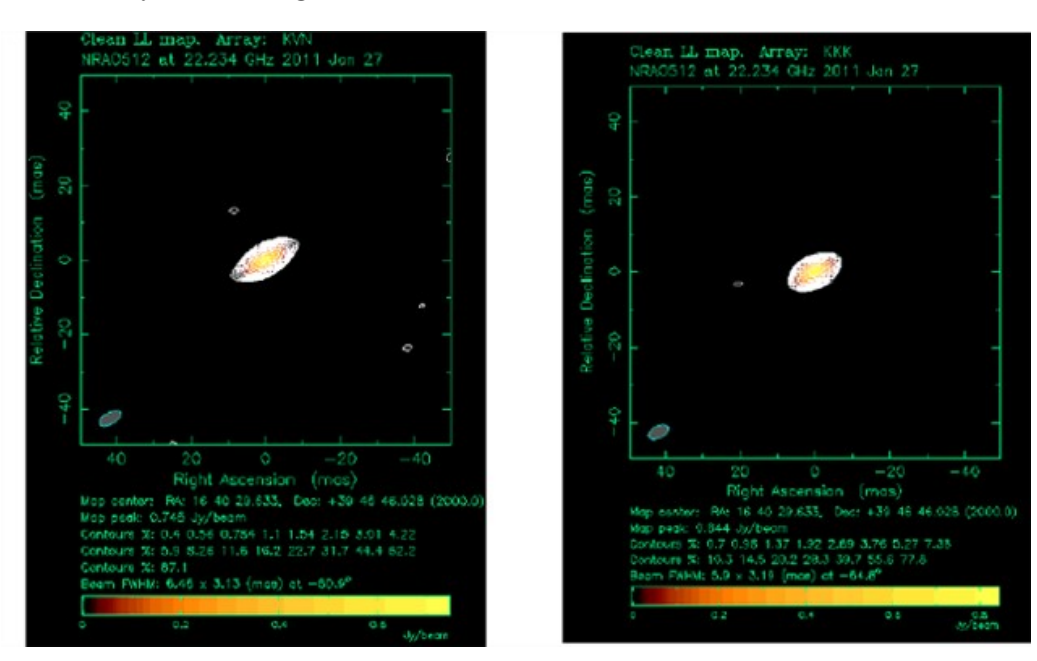


Figure 22: 2-dimensional image map using Difmap. Left (Daejeon Correlator), Right (DiFX).

In addition, we plotted the visibility with 1-dimension at UV for confirmation, as shown in Figure 23. Figure 23 shows the same result except for the difference of flux both 0.75 Jy of Daejeon Correlator and 0.84 Jy of DiFX as plotted in the above 2-dimensional map.

# Analysis result for continuum (K11017A)

Spectrum shape of raw data This experiment is to evaluate the performance of 2-frequency simultaneous observation and correlated in November 2012. 8 IFs were assigned for 22 and 43 GHz, respectively, and we report only 8 IFs for 22 GHz. We looked into the spectrum shape of POSSM after FITLD, MSORT, USUBA, and INDXR tasks. The source is NRAO530, which is a strong continuum source and is shown in Figure 24 for the KYS-KUS baseline. A phase of 8 IFs is continuously changed.

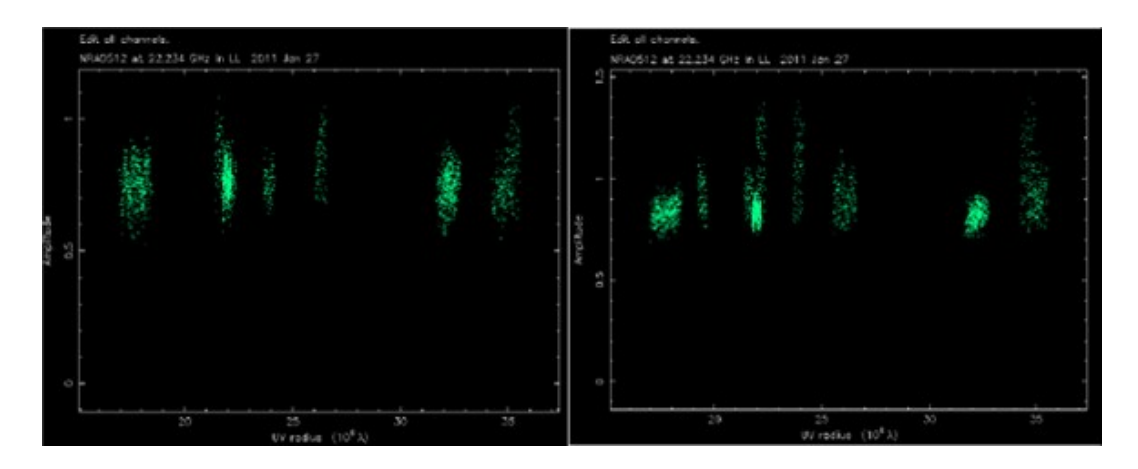


Figure 23: Flux density according to UV-distance. Left (Daejeon Correlator), Right (DiFX).

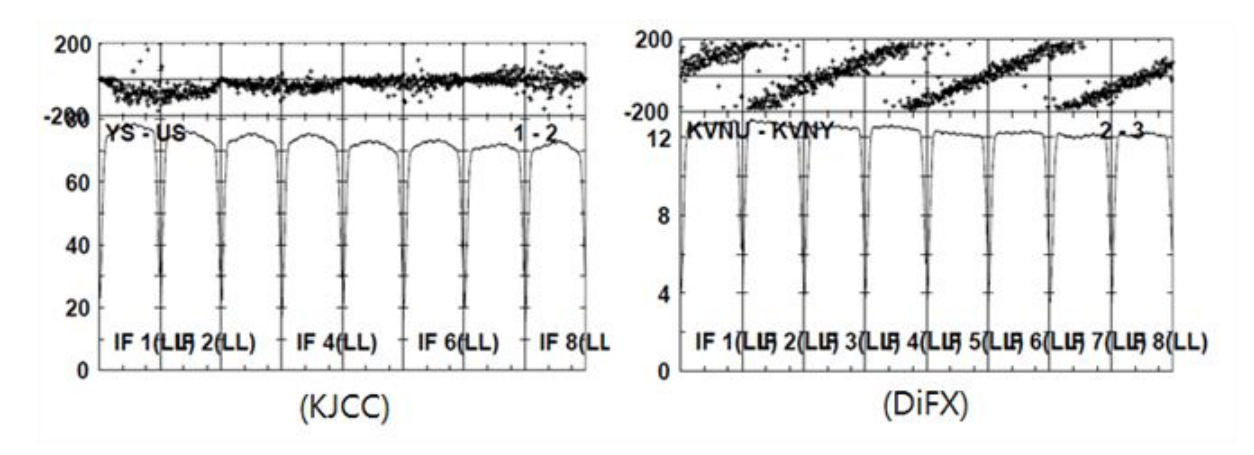


Figure 24: Spectrum shape of 8-IFs continuum for KYS-KUS baseline. Left (Daejeon Correlator), Right (DiFX).

**Gain amplitude** We looked into the gain amplitude variation of each source for the whole observation time after ACCOR as shown in Figure 25. Daejeon Correlator and DiFX had the same pattern. This observation was conducted for a long time with NRAO150 source, so the loss of  $2 \sim 4$  seconds at beginning of the scan was not affected in the correlation result.

**SNR, Delay, Rate after fringe fitting** Figure 26 shows the SNR, Delay, and Rate for each baseline, respectively. The reference was set as KVNUS. Integration time for fringe fitting is 30 seconds, SNR cutoff is 3. We used 3C454.3 which is a very strong radio source in continuum sources and the phase pattern is remarkable. For comparison with DiFX, all of the patterns for each result are almost similar without any problems.

Closure phase By using previous fringe fitting result, Closure phase for NARO150 were obtained and showed in Figure 27. We confirmed that the closure phase was about 5 degrees from calculation with a phase variation for the whole observation time and integration of  $20 \sim 109$  channels value of 1st IF for both Daejeon Correlator and DiFX.

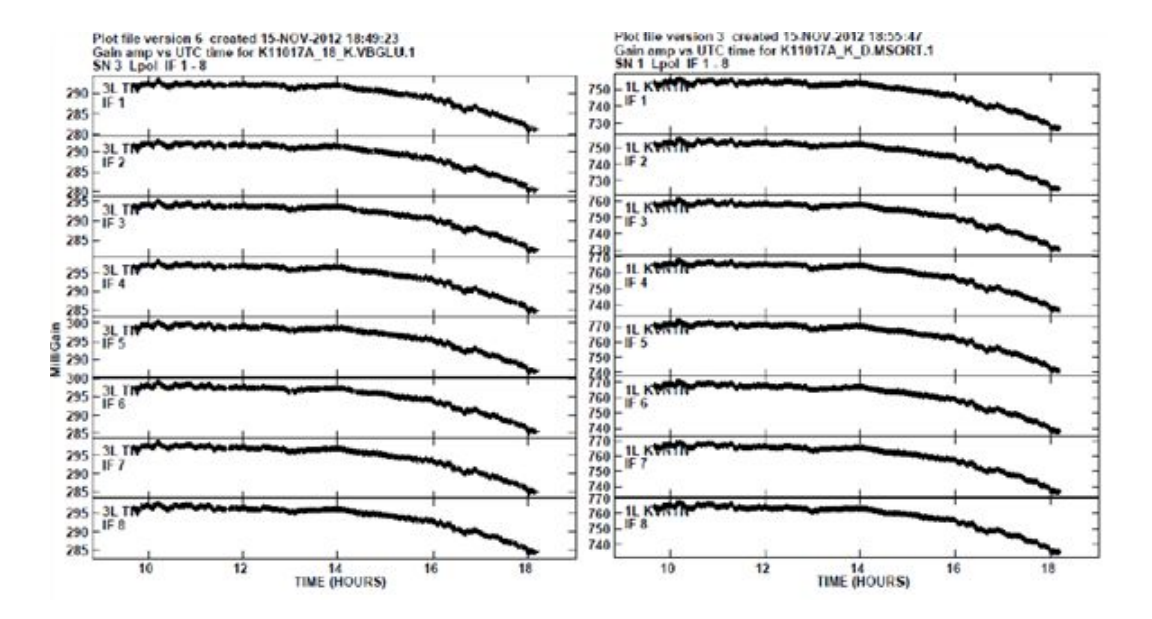


Figure 25: Variable characteristics of gain amplitude for each IF of KVNTN. Left (Daejeon Correlator), Right (DiFX).

Spectrum shape after fringe fitting and amplitude-cal. We draw again the spectrum to check phase residual by adopting the value of delay and rate after fringe fitting as shown in Figure 28. For a more detailed comparison, the range of phase was enlarged to 10 degrees and only 8 IFs were shown. Phase residual for a spectrum of Daejeon Correlator and DiFX was almost the same. To compare the flux, amplitude calibration was also applied. We confirmed that the flux of Daejeon Correlator has about 10 % lower flux than the DiFX as described in R11027B experimental result.

UV coverage, UV plot UV coverage or UV plot methods are widely used to confirm how much made up for the UV during observation of NRAO150 source. UV plot is very useful to understand the flux distribution and structure of the source. Figure 29 shows the UV coverage and UV plot for the Daejeon Correlator result. From the pattern of the UV plot, we could understand that the NRAO150 source is the bright spot with flat in KVN only baseline (less than about 30 Mega lambda).

Imaging performance A new result file was generated by averaging all IFs, all channels, and whole observation time for tables of the 3C454.3 source by using the SPLIT task. And then 2-dimensional map was plotted using a new result file as shown in Figure 30. Flux for Daejeon Correlator is 6.34 Jy/beam, which is less than about 10 % compared with 6.83 Jy/beam of DiFX, but the dynamic range is the almost same value.

#### Analysis result for spectral-line (R11027B)

**Spectrum of raw data** We confirmed the spectrum shape of the POSSM task after completion through FITLD, MSORT, USUBA, and INDXR tasks by separating only 9 IF

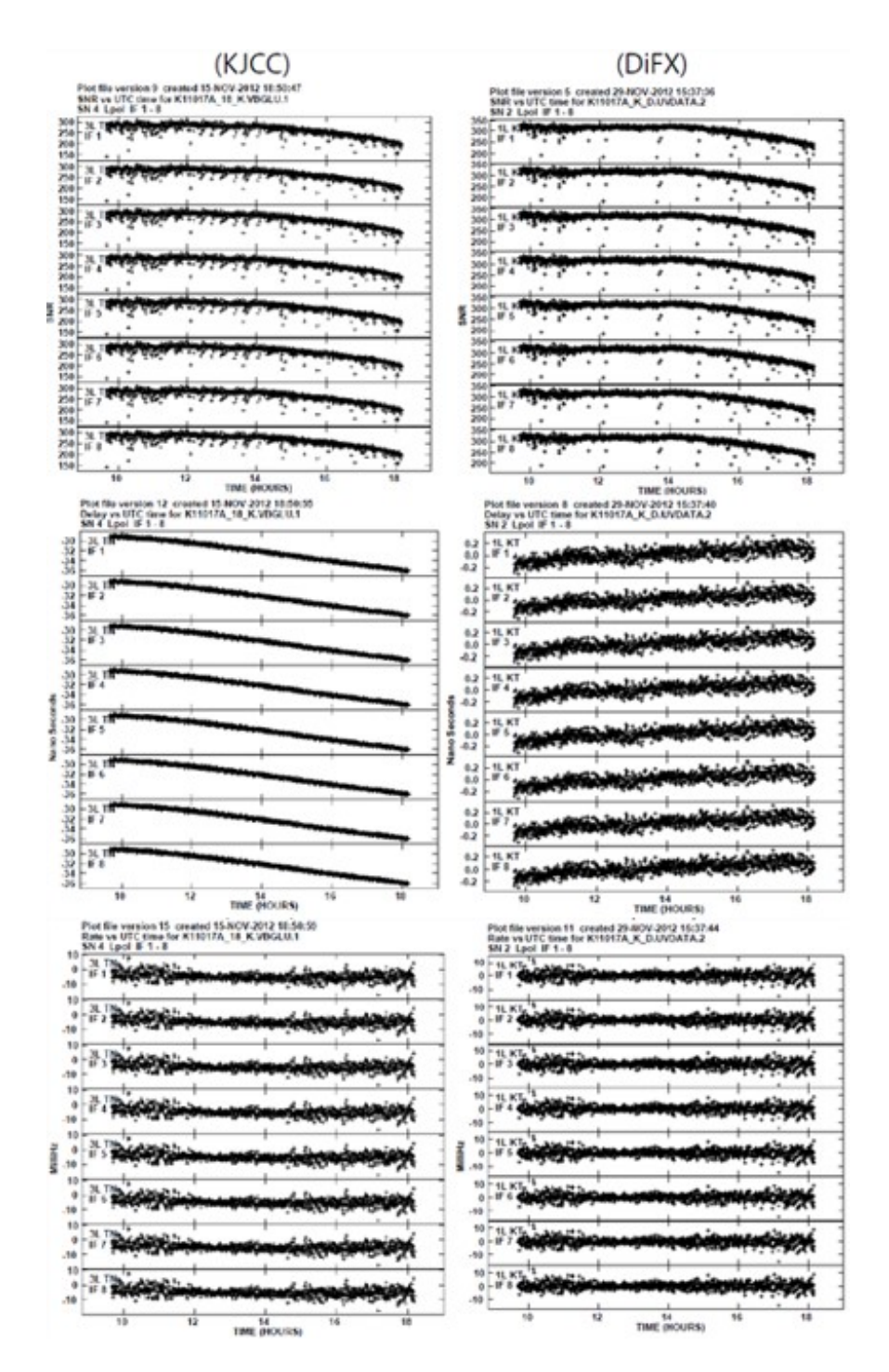


Figure 26: SNR, Delay, Rate after FRING for each IF of KTN. Left (Daejeon Correlator), Right (DiFX).

of maser source in the R11027B FITS file as shown in Figure 31. The used maser source is Sgr B2(M), which shows a strong emission line of  $22\,\mathrm{GHz}$  H<sub>2</sub>O. In the case of 9th IF, we conducted the comparison work for 3 kinds of correlators such as Daejeon Correlator, MTK, and DiFX. As you can see in Figure 28, the entire spectrum shape looks almost the

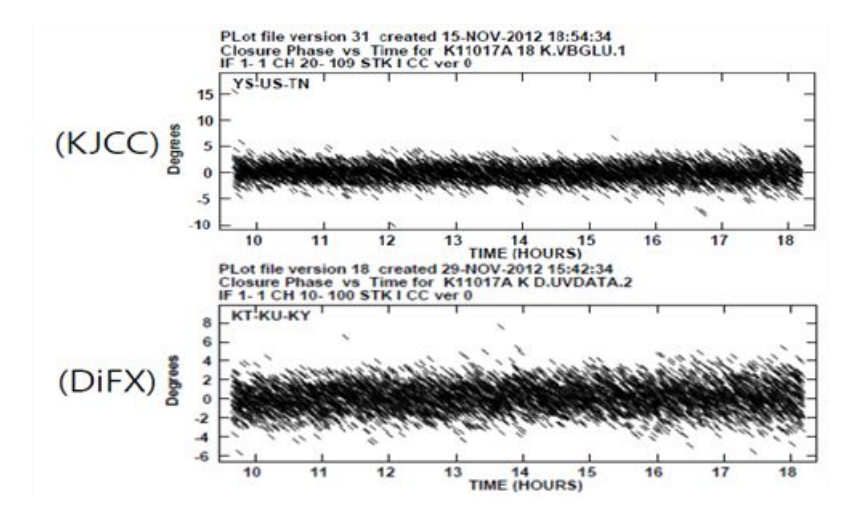


Figure 27: Closure phase after fringe fitting. Upper (Daejeon Correlator), Bottom (DiFX)

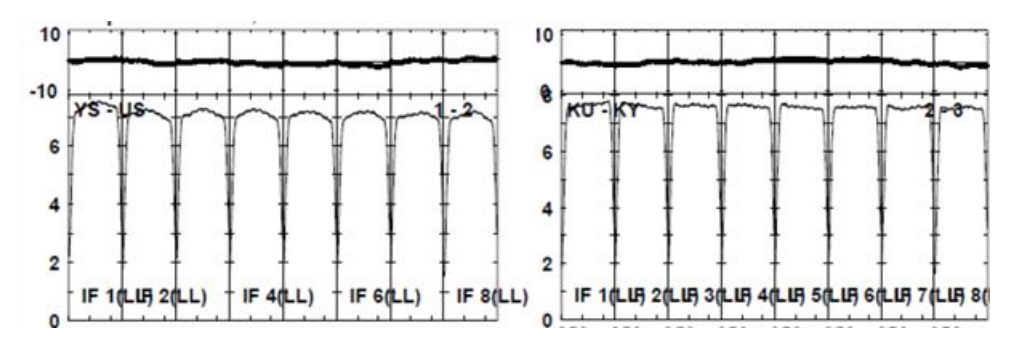


Figure 28: Closure phase after fringe fitting. Upper (Daejeon Correlator), Bottom (DiFX)

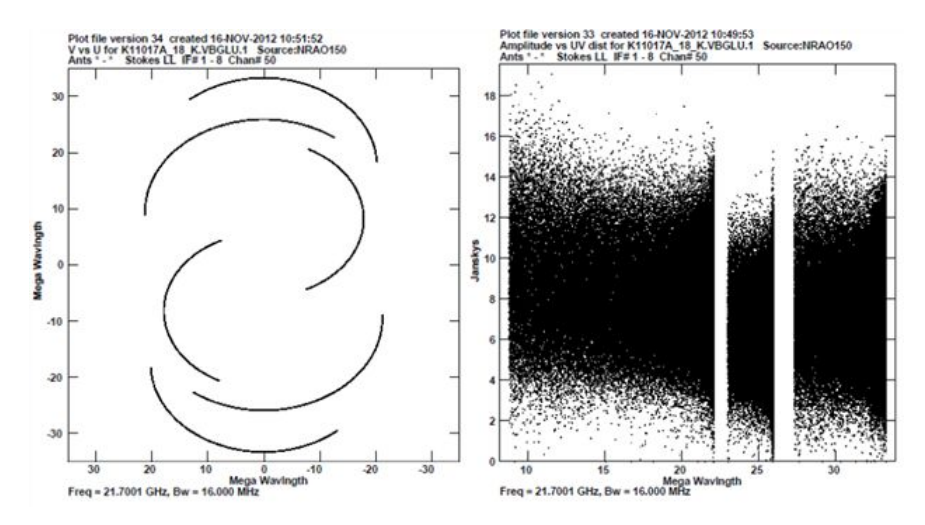


Figure 29: Closure phase after fringe fitting. Upper (Daejeon Correlator), Bottom (DiFX)

same aspect, but Daejeon Correlator has phase concentration in 0 degrees at the beginning of bandwidth because of the DC-like component. These DC-like components and phase concentration are currently disappeared.

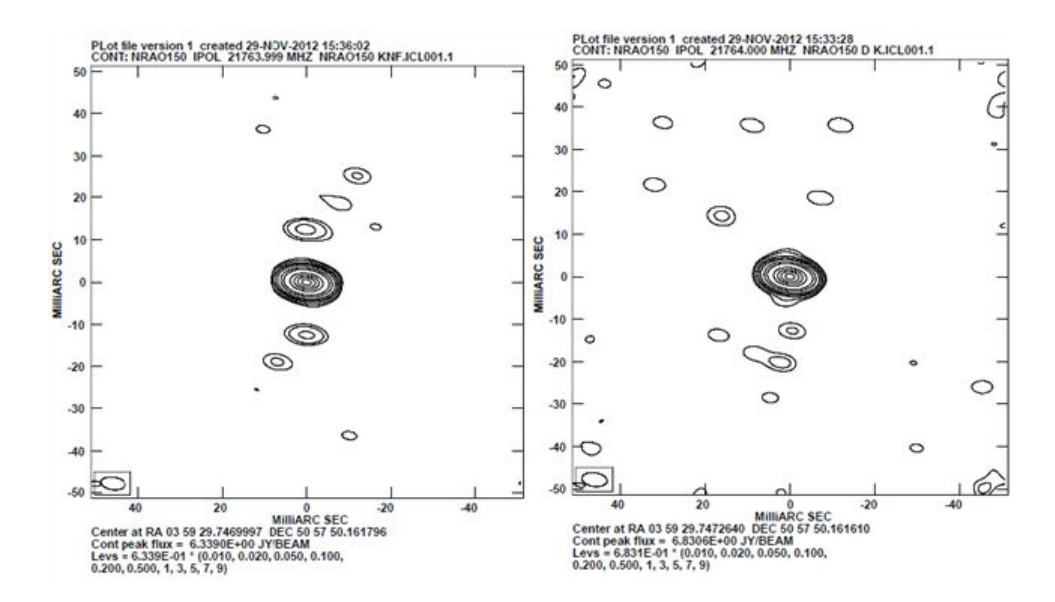


Figure 30: 2-dimensional image map using Difmap. Left (Daejeon Correlator), Right (DiFX)

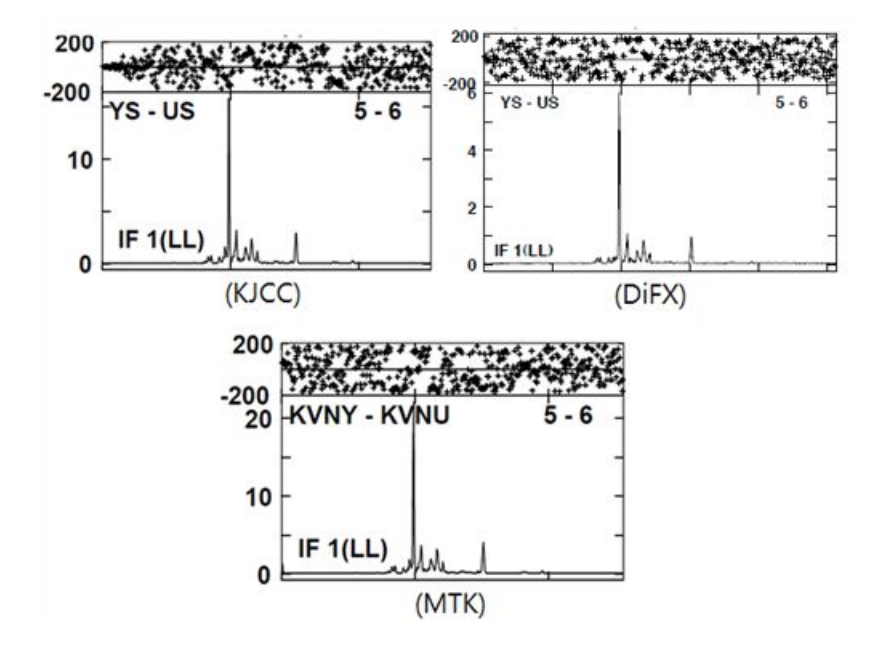


Figure 31: Spectrum shape of 9th IF of KYS and KUS baseline.

Global fringe fitting (Calibrator) Spectral-line observation such as maser source occurs the signal at very limited channel (within 10 channels) per one maser spot. Therefore, we should first apply for the clock offset compensation by performing the global fringe fitting according to the bright calibrator source because it is difficult to get the delay in the narrow frequency range. In this case, 3C345 source was used for global fringe fitting, and Figure 32 shows the delay calculated by setting the reference as KTN. Daejeon Correlator and MTK had almost the same pattern of delay because the same delay parameter was used for correlation. In the case of DiFX, it has more small delay value, and we think that this was caused by applying the more detailed clock offset compensation during the correlation

of DiFX. In Figure 32, the delay of correlation result looks good without any problem.

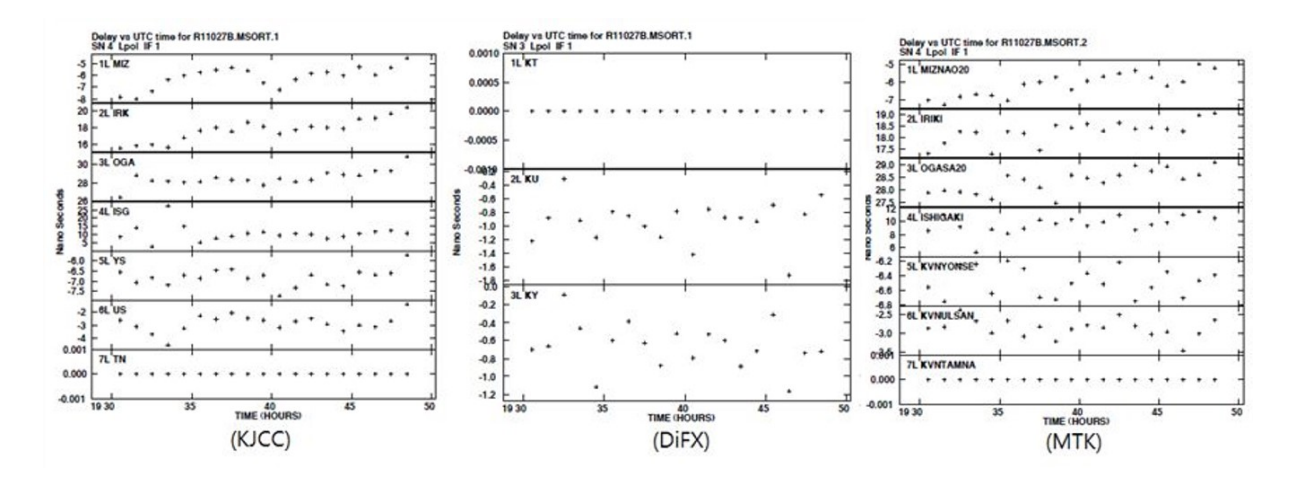


Figure 32: Fringe fitting result of 3C345 as calibrator source.

SNR after fringe fitting (maser) Fringe fitting was again conducted for the maser source by applying the delay value obtained after global fringe fitting. Although fringe fitting for continuum was done in accordance with the entire channel, fringe fitting for spectral-line was done with only one channel which has a peak value. In Figure 33, the 7th channel has strong flux, so the fringe fitting was done with this channel. Figure 33 shows the variation of SNR of the maser source for each station based on the KTN. Daejeon Correlator, MTK, and DiFX had almost the same SNR and the variation pattern also looks like the same.

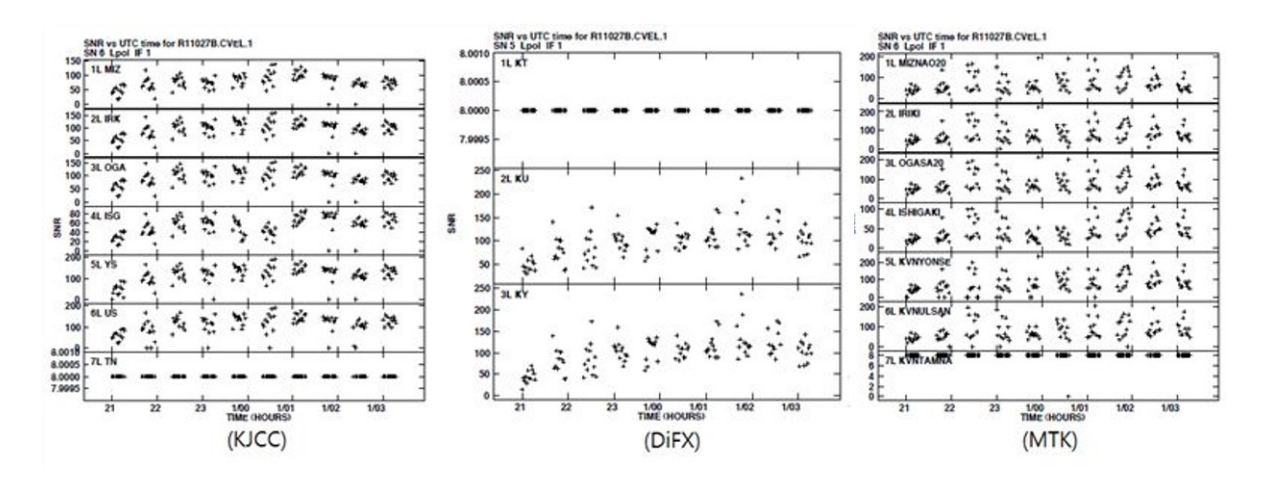


Figure 33: Fringe fitting result of Sgr B2(M) as maser source, and this figure shows SNR based on the KTN.

Spectrum shape after compensation of Dopper effect, amplitude calibration, and fringe fitting — In VLBI observation, the Dopper effect such as the earth rotation or revolution is being affected at each station. Therefore, the Dopper effect should be

compensated at the data analysis stage. CVEL command of AIPS is used for the Dopper effect compensation. Amplitude calibration was also performed so as to convert the power level to real flux value for each station. The results were shown in Figure 34. The Dopper effect was successfully compensated for the FITS file of 3 correlation results. The unit for each result is [Jy].

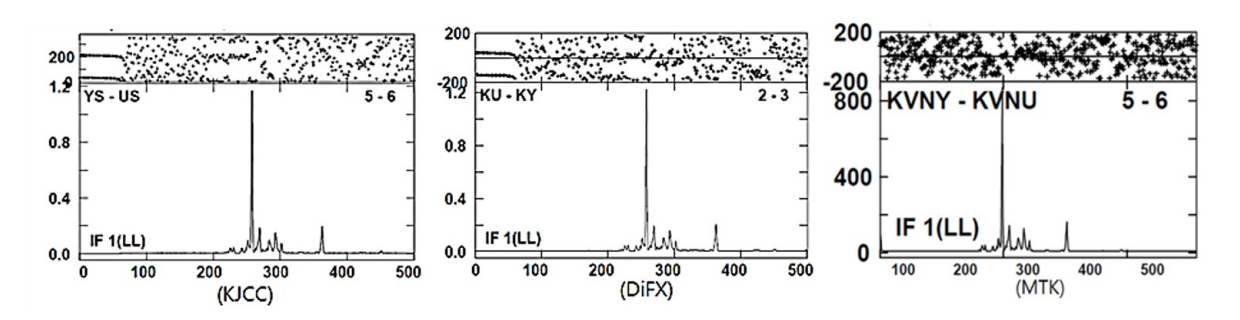


Figure 34: Spectrum shape after fringe fitting, Dopper effect, and amplitude calibration.

UV coverage, UV plot It is a very simple way to confirm the UV coverage in order to know how UV was filled during observation of the Sgr B2(M) maser source. It is helpful to know the structure and distribution of flux of source as UV-distance. Figure 35 shows the UV coverage and UV plot of correlation result with the Daejeon Correlator. From the pattern of the UV plot, Sgr B2(M) has the structure of Gaussian distribution at KaVA 7 stations, and it looks like the bright spot with flat in KVN only baseline (less than about 30 Mega lambda).

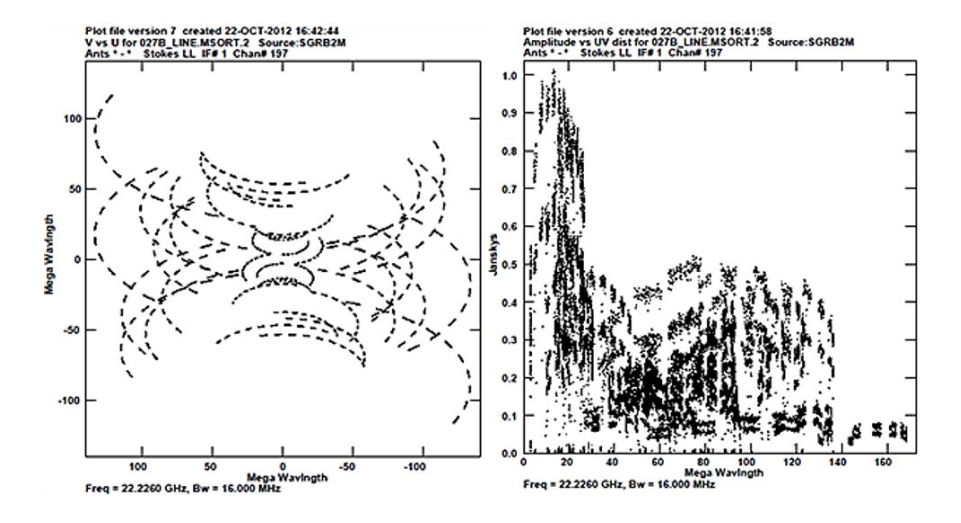


Figure 35: UV coverage (Left) and UV plot (Right) of Sgr B2(M). UV plot looks like Gaussian distribution, but KVN-only baseline seems to be flat.

Imaging performance (single channel) We conducted the imaging process with a special channel using a maser source as well as a continuum source. In the case of the

data processing stage for spectral-line, BPASS and CVEL tasks were additionally done. The resulting file was generated by applying result tables for Sgr B2(M) using the SPLIT task. For comparison with DiFX, data for KVN 3 stations were only plotted in the same way of continuum source as shown in Figure 36. Flux density for the Daejeon Correlator is about 10 % lower than the DiFX, but the dynamic range is almost the same.

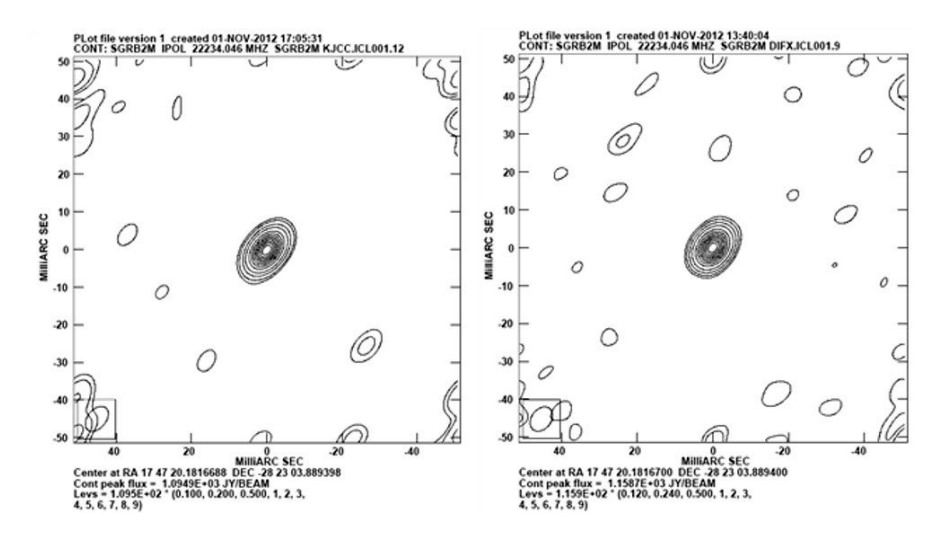


Figure 36: 2-dimensional image map using AIPS. Left (Daejeon Correlator), Right (DiFX).

Imaging performance(multi channel) In the case of maser source, maser spots exist with several tens and thousands in the uniform range. In general, imaging of the maser source is performed as follows. Firstly we find each peak channel as referring to spectrum, and then the position of whole maser spots as indicated. Finally, a 2-dimensional distribution map is plotted. In this experiment, to reproduce the image, the position was obtained by imaging for several maser spots, and then we confirmed whether the position of the maser spot for the DiFX result was consistent or not. We conducted the multi-channel imaging process as shown in Figure 37, to find the maser position, and confirmed that the maser spot for 264th, 269th, 274th, 280th, and 284th channels was detected.

#### 4.3.4 Two-layer problem had been solved

The Daejeon Correlator had solved the recent issue, named the two-layer problem. This was caused by a fault on the address set to data memory reading pointer in the data serialize FPGA part. Resultant data mixtures across the sub-bands were found out as two-layer patterns on a time-power plot, as in the left panel of Figure 38. The influence of the two-layer problem is dependent on the power difference to the first sub-band (IF1), and the loss of visibility amplitude is, very rarely, estimated as less than  $\sim 3\%$ . After fixing that fault, the visibility outputs became stable with no such pattern.

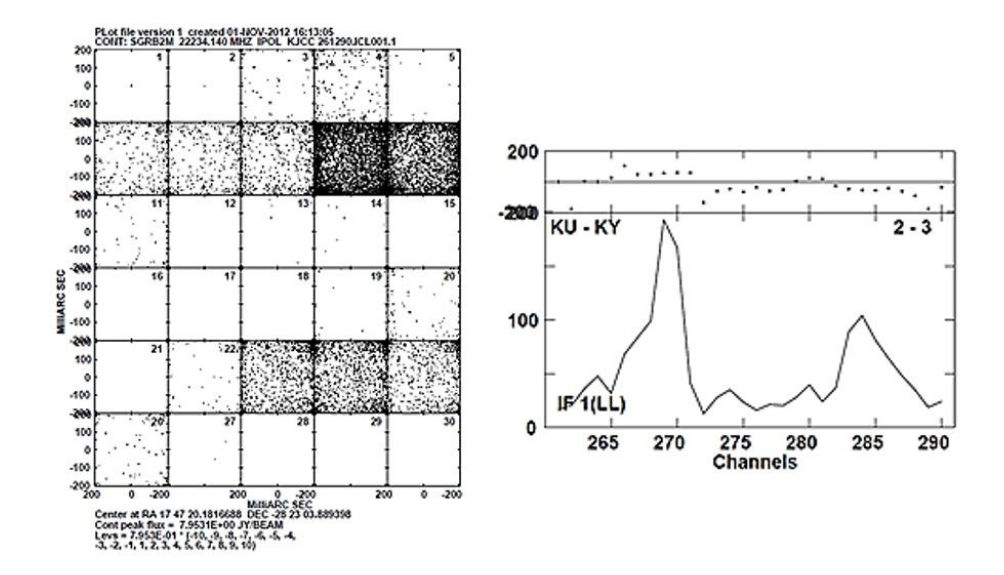


Figure 37: Example of multi-channel image. Image result for each 261th–290th channel.

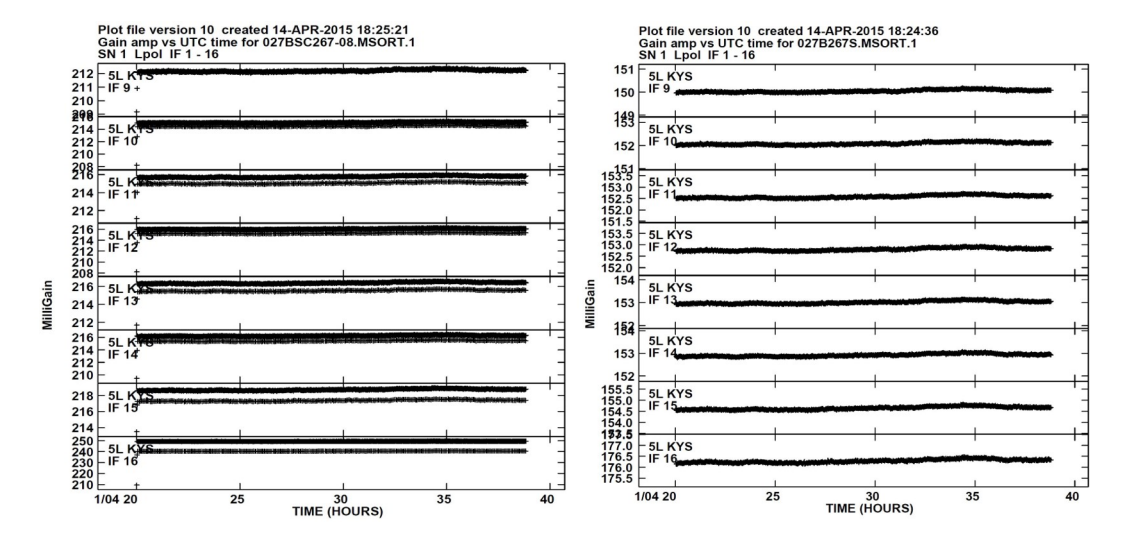


Figure 38: (Left) Before: abnormal shape with two-layer pattern, (Right) After: ordinary (as expected) shape in Gain amplitude plot (KYS, R11027B).

# 4.4 Further information

Contact address The users can contact any staff member of the KVN by e-mail (see Table 20). In addition, they will be able to obtain various information through the official webpage<sup>5</sup>.

<sup>5</sup>http://kvn.kasi.re.kr

Table 20: Contact staffs

Name	E-mail	Subject
Do-Young Byun	bdy@kasi.re.kr	Array Operation and System Specification
Sang-Sung Lee	sslee@kasi.re.kr	VLBI Performance
Taehyun Jung	thjung@kasi.re.kr	Observation Preparation and Data Analysis
Duk-Gyoo Roh	dgroh@kasi.re.kr	Correlation

# References

- [1] S.-S. Lee, L. Petrov, D.-Y. Byun, J. Kim, T. Jung, M.-G. Song, C. S. Oh, D.-G. Roh, D.-H. Je, S.-O. Wi, B. W. Sohn, S.-J. Oh, K.-T. Kim, J.-H. Yeom, M.-H. Chung, J. Kang, S.-T. Han, J.-W. Lee, B. G. Kim, H. Chung, H.-G. Kim, H. R. Kim, Y.-W. Kang, and S.-H. Cho, "EARLY SCIENCE WITH THE KOREAN VLBI NETWORK: EVALUATION OF SYSTEM PERFORMANCE," The Astronomical Journal, vol. 147, p. 77, mar 2014.
- [2] S.-T. Han, J.-W. Lee, J. Kang, D.-H. Je, M.-H. Chung, S.-O. Wi, T. Sasao, and R. Wylde, "Millimeter-wave receiver optics for korean vlbi network," *International Journal of Infrared and Millimeter Waves*, vol. 29, pp. 69–78, oct 2007.
- [3] S.-T. Han, J.-W. Lee, J. Kang, C.-S. Oh, D.-Y. Byun, D.-H. Je, M.-H. Chung, S.-O. Wi, M. Song, Y.-W. Kang, S.-S. Lee, S.-Y. Kim, T. Sasao, P. F. Goldsmith, and R. Wylde, "Korean VLBI network receiver optics for simultaneous multifrequency observation: Evaluation," *Publications of the Astronomical Society of the Pacific*, vol. 125, pp. 539–547, may 2013.
- [4] L. Petrov, S.-S. Lee, J. Kim, T. Jung, J. Oh, B. W. Sohn, D.-Y. Byun, M.-H. Chung, D.-H. Je, S.-O. Wi, M.-G. Song, J. Kang, S.-T. Han, J.-W. Lee, B. G. Kim, H. Chung, and H.-G. Kim, "EARLY SCIENCE WITH THE KOREAN VLBI NETWORK: THE QCAL-1 43 GHz CALIBRATOR SURVEY," The Astronomical Journal, vol. 144, p. 150, oct 2012.
- [5] S.-S. Lee, D.-Y. Byun, C. S. Oh, S.-T. Han, D.-H. Je, K.-T. Kim, S.-O. Wi, S.-H. Cho, B. W. Sohn, J. Kim, J. Lee, S.-J. Oh, M.-G. Song, J. Kang, M.-H. Chung, J. A. Lee, J. Oh, J.-H. Bae, S.-Y. Yun, J.-W. Lee, B. G. Kim, H. Chung, D.-G. Roh, C. H. Lee, H. G. Kim, H. R. Kim, J.-H. Yeom, T. Kurayama, T. Jung, P. Park, M. J. Kim, D.-H. Yoon, and W.-J. Kim, "Single-dish performance of KVN 21 m radio telescopes: Simultaneous observations at 22 and 43 GHz," *Publications of the Astronomical Society of the Pacific*, vol. 123, pp. 1398–1411, dec 2011.